

# Lawrence Berkeley National Laboratory

## LBL Publications

### Title

Structural Diversities in Heterometallic Mn–Ca Cluster Chemistry from the Use of Salicylhydroxamic Acid: {Mn<sup>III</sup> 4Ca<sub>2</sub>}, {Mn<sup>II/III</sup> 6Ca<sub>2</sub>}, {Mn<sup>III/IV</sup> 8Ca}, and {Mn<sup>III</sup> 8Ca<sub>2</sub>} Complexes with Relevance to Both High- and Low-Valent States of the Oxygen-Evolvi...

### Permalink

<https://escholarship.org/uc/item/8fw5p18f>

### Journal

Inorganic Chemistry, 56(17)

### ISSN

0020-1669

### Authors

Alaimo, Alysha A  
Koumoussi, Evangelia S  
Cunha-Silva, Luís  
et al.

### Publication Date

2017-09-05

### DOI

10.1021/acs.inorgchem.7b01740

Peer reviewed

Structural Diversities in Heterometallic Mn-Ca  
Cluster Chemistry from the Use of  
Salicylhydroxamic Acid: {Mn<sup>III</sup><sub>4</sub>Ca<sub>2</sub>}, {Mn<sup>II/III</sup><sub>6</sub>Ca<sub>2</sub>},  
{Mn<sup>III/IV</sup><sub>8</sub>Ca} and {Mn<sup>III</sup><sub>8</sub>Ca<sub>2</sub>} Complexes with  
Relevance to Both High- and Low-Valent States of  
the Oxygen-Evolving Complex

*Alysha A. Alaimo,<sup>†</sup> Evangelia S. Koumoussi,<sup>‡</sup> Luís Cunha-Silva,<sup>△</sup> Laura J. McCormick,<sup>#</sup> Simon J.  
Teat,<sup>#</sup> Vassilis Psycharis,<sup>§</sup> Catherine P. Raptopoulou,<sup>§</sup> Shreya Mukherjee,<sup>◇</sup> Chaoran Li,<sup>◇</sup> Sayak  
Das Gupta,<sup>◇</sup> Albert Escuer,<sup>△</sup> George Christou,<sup>◇</sup> and Theocharis C. Stamatatos<sup>\*,†</sup>*

<sup>†</sup> Department of Chemistry, Brock University, 1812 Sir Isaac Brock Way, L2S 3A1 St.  
Catharines, Ontario, Canada

<sup>‡</sup> Department of Chemistry, University of Patras, 265 04 Patras, Greece

<sup>△</sup> REQUIMTE-LAQV & Department of Chemistry and Biochemistry, Faculty of Sciences,  
University of Porto, 4169-007 Porto, Portugal

# Advanced Light Source, Lawrence Berkeley National Laboratory, 1 Cyclotron Road, Berkeley, CA 94720, USA

§ Institute of Nanoscience and Nanotechnology, NCSR “Demokritos”, 153 10 Agia Paraskevi Attikis, Greece

◇ Department of Chemistry, University of Florida, Gainesville, Florida 32611-7200, USA

▢ Departament de Química Inorgànica and Institut de Nanociència i Nanotecnologia (IN2UB), Universitat de Barcelona, Diagonal 645, 08028 Barcelona, Spain

**Corresponding Author**

\*E-mail: [tstamatatos@brocku.ca](mailto:tstamatatos@brocku.ca)

**ABSTRACT:** One-pot reactions between the  $[\text{Mn}_3\text{O}(\text{O}_2\text{CPh})_6(\text{py})_x]^{+/0}$  triangular precursors and either  $\text{CaBr}_2 \cdot x\text{H}_2\text{O}$  or  $\text{CaCl}_2 \cdot 6\text{H}_2\text{O}$ , in the presence of salicylhydroxamic acid ( $\text{shaH}_2$ ), have afforded the heterometallic complexes  $[\text{Mn}^{\text{III}}_4\text{Ca}_2(\text{O}_2\text{CPh})_4(\text{shi})_4(\text{H}_2\text{O})_3(\text{Me}_2\text{CO})]$  (**1**) and  $(\text{pyH})[\text{Mn}^{\text{II}}_2\text{Mn}^{\text{III}}_4\text{Ca}_2\text{Cl}_2(\text{O}_2\text{CPh})_7(\text{shi})_4(\text{py})_4]$  (**2**), respectively, in good yields. Further reactions but using a more flexible synthetic scheme comprising the  $\text{Mn}(\text{NO}_3)_2 \cdot 4\text{H}_2\text{O}/\text{Ca}(\text{NO}_3)_2 \cdot 4\text{H}_2\text{O}$  and  $\text{Mn}(\text{O}_2\text{CPh})_2 \cdot 2\text{H}_2\text{O}/\text{Ca}(\text{ClO}_4)_2 \cdot 4\text{H}_2\text{O}$  ‘metal blends’ and  $\text{shaH}_2$ , in the presence of external base  $\text{NEt}_3$ , led to the new complexes  $(\text{NHEt}_3)_2[\text{Mn}^{\text{III}}_4\text{Mn}^{\text{IV}}_4\text{Ca}(\text{OEt})_2(\text{shi})_{10}(\text{EtOH})_2]$  (**3**) and  $(\text{NHEt}_3)_4[\text{Mn}^{\text{III}}_8\text{Ca}_2(\text{CO}_3)_4(\text{shi})_8]$  (**4**), respectively. In all reported compounds, the anion of the tetradentate (N,O,O,O) chelating/bridging ligand salicylhydroxime ( $\text{shi}^{3-}$ ), resulted from the in-situ metal ion-assisted amide-iminol tautomerism of  $\text{shaH}_2$ , was found to bridge both Mn and Ca atoms. Complexes **1-4** exhibit a variety of different structures, metal stoichiometries, and Mn oxidation state descriptions; **1** possesses an overall octahedral metal arrangement, **2** can be described as a  $\text{Mn}_4\text{Ca}_2$  octahedron bound to an additional  $\text{Mn}_2$  unit, **3** consists of a  $\text{Mn}_8$  ‘ring’ surrounding a  $\text{Ca}^{\text{II}}$  atom, and **4** adopts a rectangular cuboidal motif of eight Mn atoms accommodating two  $\text{Ca}^{\text{II}}$  atoms. Solid-state direct current magnetic susceptibility studies revealed the presence of predominant antiferromagnetic exchange interactions between the Mn centers, leading to  $S = 0$  spin ground state values for all complexes. From a bioinorganic chemistry perspective, the reported compounds may demonstrate some relevance to both high-valent scheme (**3**) and lower oxidation level species (**1**, **2**, and **4**) of the catalytic cycle of the oxygen-evolving complex (OEC).

## INTRODUCTION

The oxygen-evolving complex (OEC) of Photosystem II (PSII) splits water into molecular O<sub>2</sub>, protons and electrons in green plants, algae, and cyanobacteria, generating the reducing equivalents and proton gradient that drive the rest of the photosynthetic process in the presence of sunlight.<sup>1</sup> Extensive research endeavors have been directed towards the synthesis of structural models (i.e., coordination compounds) that would potentially be able to mimic the structural and electronic properties of the inorganic core of OEC.<sup>2</sup> This would subsequently allow scientists to gain insight into the properties and function of the biological catalyst, as well as to understand and correlate the structural role of several components (i.e., metal ions, ligands, etc.) with the activity of the native enzyme itself towards the development of artificial photosynthesis.<sup>3</sup>

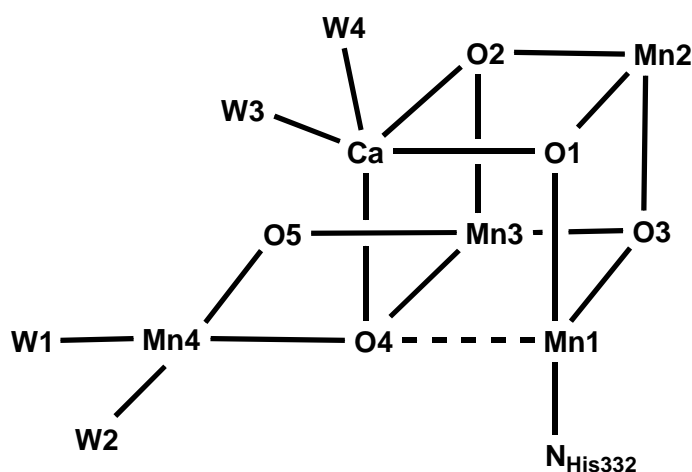
The OEC contains a heterometallic {Mn<sub>4</sub>CaO<sub>5</sub>} cluster (Scheme 1),<sup>4</sup> also known as the water-oxidizing complex (WOC), which consists of an oxido-bridged {Mn<sub>3</sub>CaO<sub>4</sub>} distorted cubane unit linked to a fourth, dangling Mn atom through one of the unit's oxido bridges and an additional bis-μ-O<sup>2-</sup> group (O5; Scheme 1). Peripheral ligation about the overall {Mn<sub>4</sub>CaO<sub>5</sub>} core is mostly provided by aspartate and glutamate carboxylate groups of various polypeptide moieties, as well as one histidine (N<sub>His332</sub>) and four water molecules or water-derived ligands (W1-W4; Scheme 1).<sup>5</sup> X-ray absorption spectroscopy (XAS), including extended X-ray absorption fine structure (EXAFS) and X-ray absorption near edge spectroscopy (XANES), have been invaluable tools in assessing the metal topology, stoichiometry and distances between atoms that compose the OEC.<sup>6</sup> These studies, along with EPR spectroscopy,<sup>7</sup> have allowed for the description of the Mn oxidation states at each of the *S* states (*S<sub>n</sub>*, where *n* = 0-4) of the catalytic Kok cycle, where the subscript indicates the number of stored oxidizing equivalents.<sup>8</sup> The Mn ions at the various *S<sub>n</sub>* Kok states exist in high oxidation states and are described as a

mixture of  $\text{Mn}^{\text{III}}$ ,  $\text{Mn}^{\text{IV}}$ , and probably  $\text{Mn}^{\text{V}}$ .<sup>1,2,9</sup> The  $S_0$  state is  $3\text{Mn}^{\text{III}}/1\text{Mn}^{\text{IV}}$ , the dark-stable  $S_1$  state is  $2\text{Mn}^{\text{III}}/2\text{Mn}^{\text{IV}}$ , the  $S_2$ , which is probably the most studied Kok state, is  $\text{Mn}^{\text{III}}/3\text{Mn}^{\text{IV}}$ , the metastable  $S_3$  state has a  $4\text{Mn}^{\text{IV}}$  or  $\text{Mn}^{\text{III}}/3\text{Mn}^{\text{IV}}$ -ligand radical description, and the transient  $S_4$  state is either a  $4\text{Mn}^{\text{IV}}$ -ligand radical description or  $3\text{Mn}^{\text{IV}}/\text{Mn}^{\text{V}}$ .<sup>10</sup> During the fourth oxidation,  $\text{O}_2$  is evolved and the catalyst is reset to the  $S_0$  state. In addition, the presence of  $\text{Ca}^{\text{II}}$  atom is very important for the activity of the OEC; without its existence, the OEC could not advance to the metastable  $S_3$  state.<sup>11</sup> Substitution of other metal ions for  $\text{Ca}^{\text{II}}$  leads to inhibition of the catalytic activity, except for  $\text{Sr}^{\text{II}}$ , which partially recovers activity.<sup>12</sup> Furthermore, the first atomic-resolution ( $1.9 \text{ \AA}$ ) model of the native OEC by Umena and coworkers<sup>13</sup> revealed the presence of two  $\text{Cl}^-$  atoms in the vicinity of the  $\{\text{Mn}_4\text{Ca}\}$  cluster, as well as one bicarbonate ion in close proximity. These anions have mainly a structural role and they serve to stabilize the catalytic center of the OEC. In contrast, the coordinated oxido groups appear to have a more crucial role in the stabilization of the high Mn oxidation states, the satisfaction of the  $\text{Ca}^{\text{II}}$  oxophilicity, and eventually the assembly of the five metal ions into the extended, distorted cubane topology of the OEC.<sup>14</sup> Oxides are usually generated from the complete deprotonation of water molecules; the process by which the OEC is assembled, called photoactivation, utilizes Mn, Ca,  $\text{Cl}^-$ ,  $\text{H}_2\text{O}$ , and oxidizing equivalents resulted from light absorption.<sup>15</sup>

The determination of kinetically distinct species during the photoactivation process and the reduction of the  $S_n$  intermediates in the Kok cycle have led to species in oxidation states lower than  $S_0$ , which do not require the presence of oxido groups;<sup>16</sup> these  $S_n$  states ( $n = -1, -2, -3$ ) are known as the reduced OEC states and contain Mn ions in lower oxidation states (i.e.,  $\text{Mn}^{\text{II}}$ ,  $\text{Mn}^{\text{III}}$ ).<sup>17</sup> During the catalytic turnover, lower oxidation state species with lower oxygen-atom content must be generated upon loss of molecular  $\text{O}_2$ .<sup>18</sup> The ligand set environment is then

responsible for the periodic reorganization, reoxidation, and reoxygenation of the  $\{\text{Mn}_4\text{CaO}_x\}$  cluster.<sup>19</sup> Therefore, the synthesis and detailed study of synthetic analogues of the OEC containing Mn ions in the 2+/3+ oxidation states would also be interesting and would greatly enhance our understanding of the spectroscopic, physical and catalytical properties of the WOC, as well as its reactivity and functional characteristics.

**Scheme 1. Latest model for the  $\{\text{Mn}_4\text{CaO}_5\}$  Cluster of the OEC Core in Photosystem II**



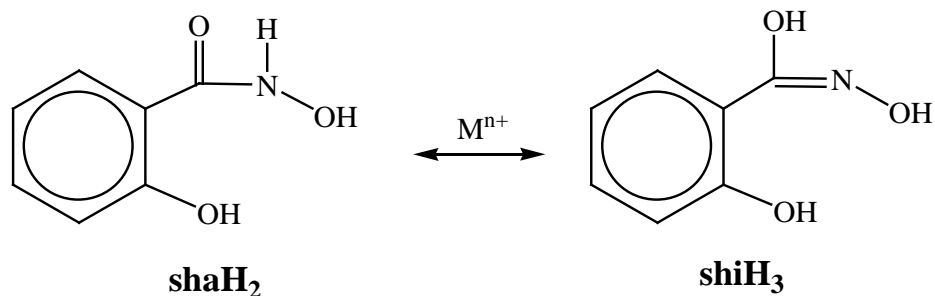
Although multinuclear, homometallic Mn clusters at various oxidation state levels and descriptions have been extensively reported over the last two decades or so,<sup>20</sup> heterometallic Mn-Ca molecular cluster chemistry has been only sparingly developed.<sup>21</sup> Agapie,<sup>22</sup> Zhang,<sup>23</sup> and a few of us,<sup>24</sup> have reported some of the closest structural models to the native OEC core, all containing the desired  $\{\text{Mn}_3\text{CaO}_4\}$  cubane core and Mn atoms in high oxidation states (i.e.,  $\text{Mn}^{\text{IV}}$ ). In all cases, different chelating and bridging ligands have been utilized, including carboxylates and pyridyl polyalcohols, among others. These molecular compounds nicely resemble some of the latter *S* states ( $S_2$  and  $S_3$ ) of the catalytic Kok cycle within the native OEC.

Along these lines, Pantazis and coworkers have recently reviewed the individual or combined synthetic targets for the structural biomimetic chemistry of the OEC.<sup>25</sup>

We have recently started a program aiming at the exploration of the low oxidation states ( $S_n$  states;  $n = -1, -2, -3$ ) of the catalytic cycle through the synthesis of heterometallic Mn-Ca complexes with unique structural motifs, diverse topologies and different Mn oxidation state descriptions that would not require for their stabilization and crystallization to occur in the presence of bridging oxido groups.<sup>26</sup> Following up with the elegant work of Pecoraro and coworkers in  $3d$ - and  $3d/4f$ -metal chemistry,<sup>27</sup> we have also shown that salicylhydroxamic acid (shaH<sub>2</sub>, Scheme 2), a photosynthetically effective group,<sup>28</sup> can undergo a metal-assisted amide-iminol tautomerism, which leads to the ligand salicylhydroxime (shiH<sub>3</sub>, Scheme 2). The latter is an oximate-based ligand with four coordination sites available for binding to both Mn and Ca metal centers. The employment of salicylhydroxime in Mn-Ca chemistry has previously led us to the synthesis of the first family of oxido-free {Mn<sup>III</sup><sub>4</sub>Ca} complexes with a square pyramidal topology and the exact metal stoichiometry as that found in the native OEC.<sup>26</sup> In this work, we have discovered new synthetic conditions to unveil four different heterometallic Mn-Ca/shi<sup>3-</sup> complexes with diverse nuclearities, metal stoichiometries and oxidation state descriptions of relevance to both high- and low-oxidation states of the OEC. The synthesis, structures and magnetic properties of the heterometallic {Mn<sup>III</sup><sub>4</sub>Ca<sub>2</sub>}, {Mn<sup>II/III</sup><sub>6</sub>Ca<sub>2</sub>}, {Mn<sup>III/IV</sup><sub>8</sub>Ca} and {Mn<sup>III</sup><sub>8</sub>Ca<sub>2</sub>} complexes are reported herein.

**Scheme 2. Metal-Assisted Amide-Iminol Tautomerism of Salicylhydroxamic Acid (shaH<sub>2</sub>) to Salicylhydroxime (shiH<sub>3</sub>)**





## EXPERIMENTAL SECTION

**Synthesis.** All manipulations were performed under aerobic conditions using chemicals and solvents as received, unless otherwise stated. The starting materials  $\text{Mn}(\text{O}_2\text{CPh})_2 \cdot 2\text{H}_2\text{O}$ ,  $[\text{Mn}_3\text{O}(\text{O}_2\text{CPh})_6(\text{py})_3](\text{ClO}_4)$  and  $[\text{Mn}_3\text{O}(\text{O}_2\text{CPh})_6(\text{py})_2(\text{H}_2\text{O})]$  (py = pyridine) were prepared as described elsewhere.<sup>29</sup> *Perchlorate salts are potentially explosive; such compounds should be synthesized and used in small quantities, and treated with utmost care at all times.*

**$[\text{Mn}_4\text{Ca}_2(\text{O}_2\text{CPh})_4(\text{shi})_4(\text{H}_2\text{O})_3(\text{Me}_2\text{CO})]$  (1).** To a stirred, colorless solution of shaH<sub>2</sub> (0.31 g, 2.0 mmol) in Me<sub>2</sub>CO (30 mL) the solids  $[\text{Mn}_3\text{O}(\text{O}_2\text{CPh})_6(\text{py})_3](\text{ClO}_4)$  (0.87 g, 0.7 mmol) and CaBr<sub>2</sub>·xH<sub>2</sub>O (0.20 g, 1.0 mmol) were added together. The resulting brown suspension was stirred for 1 h, during which time all the solids dissolved, and the color of the solution changed to dark brown. The solution was filtered and left to evaporate slowly at room temperature. After five days, brown plate-like crystals of **1**·3Me<sub>2</sub>CO·2.8H<sub>2</sub>O appeared and were collected by filtration, washed with Me<sub>2</sub>CO (2 × 5 mL) and Et<sub>2</sub>O (2 × 5 mL), and dried in air; the yield was 60%. The crystalline solid was analyzed as **1**·2H<sub>2</sub>O: C, 46.23; H, 3.42; N, 3.65 %. Found: C, 46.43; H, 3.58; N, 3.54 %. Selected ATR data (cm<sup>-1</sup>): 3058 (wb), 1595 (s), 1567 (s), 1543 (m), 1509 (s),

1432 (m), 1389 (vs), 1316 (s), 1244 (m), 1157 (m), 1100 (m), 1068 (w), 1023 (m), 929 (s), 864 (w), 838 (w), 749 (w), 721 (vs), 678 (vs), 648 (s), 602 (vs), 531 (w), 477 (s), 408 (m).

**(pyH)[Mn<sub>6</sub>Ca<sub>2</sub>Cl<sub>2</sub>(O<sub>2</sub>CPh)<sub>7</sub>(shi)<sub>4</sub>(py)<sub>4</sub>] (2).** To a stirred, colorless suspension of shaH<sub>2</sub> (0.08 g, 0.5 mmol) in CH<sub>2</sub>Cl<sub>2</sub> (30 mL) the solids [Mn<sub>3</sub>O(O<sub>2</sub>CPh)<sub>6</sub>(py)<sub>2</sub>(H<sub>2</sub>O)] (0.54 g, 0.5 mmol) and CaCl<sub>2</sub>·6H<sub>2</sub>O (0.11 g, 0.5 mmol) were added together. The resulting red suspension was stirred for 2 h, during which time all the solids dissolved, and the color of the solution changed to brown. The solution was filtered, and Et<sub>2</sub>O (60 mL) diffused into the filtrate. After ten days, red rod-like crystals of **2**·2Et<sub>2</sub>O·CH<sub>2</sub>Cl<sub>2</sub> appeared and were collected by filtration, washed with CH<sub>2</sub>Cl<sub>2</sub> (2 × 5 mL) and Et<sub>2</sub>O (2 × 5 mL), and dried in air; the yield was 45%. The crystalline solid was analyzed as solvent-free **2**: C, 52.68; H, 3.34; N, 5.42 %. Found: C, 52.59; H, 3.25; N, 5.64 %. Selected ATR data (cm<sup>-1</sup>): 3041 (m), 1597 (s), 1569 (s), 1512 (m), 1487 (m), 1468 (m), 1445 (m), 1432 (m), 1393 (vs), 1359 (s), 1319 (s), 1250 (m), 1218 (m), 1176 (m), 1099 (m), 1067 (m), 1037 (s), 927 (s), 865 (s), 838 (m), 754 (m), 719 (vs), 672 (vs), 647 (s), 475 (vs), 434 (m).

**(NHEt<sub>3</sub>)<sub>2</sub>[Mn<sub>8</sub>Ca(OEt)<sub>2</sub>(shi)<sub>10</sub>(EtOH)<sub>2</sub>] (3).** To a stirred, colorless solution of shaH<sub>2</sub> (0.08 g, 0.5 mmol) and NEt<sub>3</sub> (0.21 mL, 1.5 mmol) in EtOH (30 mL) the solids Mn(NO<sub>3</sub>)<sub>2</sub>·4H<sub>2</sub>O (0.13 g, 0.5 mmol) and Ca(NO<sub>3</sub>)<sub>2</sub>·4H<sub>2</sub>O (0.12 g, 0.5 mmol) were added together. The resulting dark red suspension was stirred for 1 h, during which time all the solids dissolved and the color of the solution changed to very dark brown. The solution was filtered and left to evaporate slowly at room temperature. After two weeks, dark-brown plate-like crystals of **3**·3EtOH·H<sub>2</sub>O appeared and were collected by filtration, washed with cold EtOH (2 × 5 mL) and Et<sub>2</sub>O (2 × 5 mL), and dried in air; the yield was 30%. The crystalline solid was analyzed as **3**·2H<sub>2</sub>O: C, 43.86; H, 4.19; N, 7.14 %. Found: C, 43.71; H, 4.12; N, 7.22 %. Selected ATR data (cm<sup>-1</sup>): 3375 (mb), 3062

(m), 2966 (mb), 1595 (s), 1564 (s), 1471 (vs), 1384 (vs), 1314 (vs), 1257 (s), 1153 (m), 1098 (m), 1034 (s), 950 (s), 860 (s), 752 (s), 672 (vs), 641 (s), 591 (sb), 461 (m).

**(NH<sub>4</sub>)<sub>4</sub>[Mn<sub>8</sub>Ca<sub>2</sub>(CO<sub>3</sub>)<sub>4</sub>(shi)<sub>8</sub>] (4).** To a stirred, colorless solution of shaH<sub>2</sub> (0.08 g, 0.5 mmol) and NEt<sub>3</sub> (0.21 mL, 1.5 mmol) in CHCl<sub>3</sub> (30 mL) the solids Mn(O<sub>2</sub>CPh)<sub>2</sub>·2H<sub>2</sub>O (0.17 g, 0.5 mmol) and Ca(ClO<sub>4</sub>)<sub>2</sub>·4H<sub>2</sub>O (0.16 g, 0.5 mmol) were added together. The resulting dark red suspension was stirred for 3 h, during which time all the solids dissolved and the color of the solution changed to dark brown. The solution was filtered and left to evaporate slowly at room temperature. After one month, brown plate-like crystals of **4**·9CHCl<sub>3</sub> appeared and were collected by filtration, washed with CHCl<sub>3</sub> (2 × 5 mL) and Et<sub>2</sub>O (2 × 5 mL), and dried under vacuum; the yield was 20%. The crystalline solid was analyzed as **4**·2CHCl<sub>3</sub>: C, 40.22; H, 3.85; N, 6.54 %. Found: C, 40.36; H, 3.99; N, 6.48 %. Selected ATR data (cm<sup>-1</sup>): 2993 (mb), 1595 (s), 1566 (s), 1508 (s), 1468 (m), 1448 (m), 1432 (s), 1375 (vs), 1316 (s), 1255 (s), 1155 (m), 1098 (m), 1066 (m), 1027 (s), 935 (s), 863 (s), 749 (vs), 720 (vs), 673 (vs), 645 (vs), 609 (vs), 532 (m), 443 (s), 415 (m).

**X-ray Crystallography.** A brown single-crystal of complex **1**·3Me<sub>2</sub>CO·2.8H<sub>2</sub>O was mounted in capillary with drops of mother liquid because they were destroyed immediately when immersed into the crystallographic oil; this was confirmed by the presence of many partially occupied solvate molecules. Diffraction measurements were made at room temperature on a Rigaku R-Axis SPIDER Image Plate diffractometer using graphite-monochromated Cu K $\alpha$  radiation. Data collection ( $\omega$ -scans) and processing (cell refinement, data reduction and empirical absorption correction) were performed using the CrystalClear program package.<sup>30</sup> The structure was solved by direct methods using SHELXS-97,<sup>31,38</sup> and refined by full-matrix least-squares techniques on  $F^2$  with SHELXL ver. 2014/6.<sup>32</sup> All non-H atoms were refined anisotropically,

except from those belonging to partially occupied solvate molecules which were refined isotropically. All H atoms were introduced at calculated positions as riding on their respective atoms. No H atoms for the partially occupied solvate molecules were included in the refinement. The O2W and O41 atoms that belong to the coordinated H<sub>2</sub>O and acetone molecules are disordered with site occupancies of 0.5.

Data for complexes **2**·2Et<sub>2</sub>O·CH<sub>2</sub>Cl<sub>2</sub> and **3**·3EtOH·H<sub>2</sub>O were collected on beamline 11.3.1 at the Advanced Light Source, Lawrence Berkeley National Lab. Samples were mounted on MiTeGen® kapton loops and placed in a 100(2) K nitrogen cold stream provided by an Oxford Cryostream 700 Plus low temperature apparatus on the goniometer head of a Bruker D8 diffractometer equipped with a PHOTON100 CMOS detector operating in shutterless mode. Diffraction data were collected using monochromated synchrotron radiation (silicon(111) to a wavelength of 0.8856(1) Å and 0.7749(1) Å for **2** and **3**, respectively). An approximate full-sphere of data was collected using a combination of phi and omega scans with scan speeds of 1 second per 4 degrees for the phi scans, and 1 and 3 seconds per degree for the omega scans at  $2\theta = 0$  and  $-45$ , respectively. The structures were solved by intrinsic phasing (SHELXT) and refined by full-matrix least squares on  $F^2$  (SHELXL-2014). All non-hydrogen atoms were refined anisotropically. Hydrogen atoms were geometrically calculated and refined as riding atoms. For complex **2**, the coordinated pyridine molecules were found to be disordered and the carbon atoms have been modelled over two sites with complementary occupancies. Some minor rotational disorder was also found for the aromatic rings of the shi<sup>3-</sup> and PhCO<sub>2</sub><sup>-</sup> groups. The free pyridinium cation is rotationally disordered over two sites, such that the -NH group can occupy one of the two symmetry-related sites. The carbon and nitrogen atoms that occupy this site have been refined with occupancies of 0.5, with the same *xyz* coordinates and isotropic displacement

parameters as each other. The partial occupancy of the CH<sub>2</sub>Cl<sub>2</sub> molecule was found to be disordered over two symmetry-related sites, and the atoms were refined isotropically with site occupancies of 0.5. The C3E-C4E ethyl chain of the Et<sub>2</sub>O molecule was found to be disordered; however, only the major orientation of this chain could be modelled satisfactorily (occupancy 0.81). For complex **3**, all non-hydrogen atoms belonging to the cluster were located. The aromatic ring of one shi<sup>3-</sup> ligand was found to be disordered and has been modelled over two sites with complementary site occupancies. In addition to the cluster compound, there are two triethylammonium (NHET<sub>3</sub><sup>+</sup>) cations, three guest ethanol molecules and a water molecule. The two NHET<sub>3</sub><sup>+</sup> cations were found to be disordered and have been modelled over two locations. Similarly, the ethanol molecules were each found to be disordered and have been modelled over two or three different positions. Equivalent atoms have been constrained to have equal  $U_{ij}$  values. Different orientations of the same molecule have been restrained to have equal bond lengths and angles by use of the RESI and SAME commands. The ammonium hydrogen atom belonging to the minor orientation of the N1a cation has been held in place by use of SDAI commands keeping an equal distance between the hydrogen atom and the three carbon atoms bound to the central nitrogen atom. All ammonium and hydroxido hydrogen atoms were located at the difference map, fixed at distances of 0.88 and 0.84 Å from the nitrogen or oxygen atoms, respectively, to which they are bound, and given a thermal displacement parameter of 1.2 or 1.5 times that of the corresponding N or O atom to which they are bound. Not all hydroxido or water hydrogen atoms could be located during the refinement. These ‘missing’ hydrogen atoms have been included in the molecular formula but not in the final model.

A selected crystal of complex **4**·9CHCl<sub>3</sub> was manually harvested and mounted on a cryoloop using adequate oil.<sup>33</sup> All the single-crystals chosen for data collection showed very weak X-ray

diffraction patterns under the accessible Mo K $\alpha$  radiation. It was not feasible to obtain any better diffraction for this complex, but the reported data are of enough quality to adequately confirm the metals' connectivity and most of the molecules in the crystal lattice. Diffraction data were collected at 150.0(2) K on a Bruker X8 Kappa APEX II Charge-Coupled Device (CCD) area-detector diffractometer controlled by the APEX2 software package<sup>34</sup> (Mo K $\alpha$  graphite-monochromated radiation,  $\lambda = 0.71073 \text{ \AA}$ ), and equipped with an Oxford Cryosystems Series 700 cryostream monitored remotely with the software interface Cryopad.<sup>35</sup> Images were processed with the software SAINT+,<sup>36</sup> and absorption effects corrected with the multiscan method implemented in SADABS.<sup>37</sup> The structure was solved using the algorithm implemented in SHELXT-2014,<sup>38,39</sup> and refined by successive full-matrix least-squares cycles on  $F^2$  using the latest SHELXL-v.2014.<sup>38,40</sup> The non-hydrogen atoms were successfully refined using anisotropic displacement parameters. Hydrogen atoms bonded to carbon were placed at their idealized positions using the appropriate HFIX instructions in SHELXL and included in subsequent refinement cycles in riding-motion approximation with isotropic thermal displacements parameters ( $U_{iso}$ ) fixed at 1.2 or  $1.5 \times U_{eq}$  of the relative atom. Considerable electron density was found on the data of the crystal structure, probably due to additional disordered solvate molecules occupying the spaces created by the packing arrangement of the complexes. Efforts to accurately locate, model and refine these residues turned to be ineffective, and the investigation for the total potential solvent area using the software package PLATON<sup>41a,b</sup> confirmed the existence of cavities with potential solvent accessible void volume. Thus, the original data sets were treated with the program SQUEEZE,<sup>41c</sup> which calculates the contribution of the smeared electron density in the lattice voids and adds this to the calculated structure factors from the structural model when refining against the hkl file.

The programs used for molecular graphics were MERCURY<sup>41d</sup> and DIAMOND.<sup>41e</sup> Unit cell parameters and structure solution and refinement data for all complexes are listed in Table 1. Further crystallographic details can be found in the corresponding CIF files provided in the Supporting Information.

**Table 1. Crystallographic Data for Complexes 1-4**

Parameter	1·3Me <sub>2</sub> CO·2.8H <sub>2</sub> O	2·2Et <sub>2</sub> O·CH <sub>2</sub> Cl <sub>2</sub>	3·3EtOH·H <sub>2</sub> O	4·9CHCl <sub>3</sub>
Formula <sup>a</sup>	C <sub>68</sub> H <sub>71.6</sub> Mn <sub>4</sub> Ca <sub>2</sub> N <sub>4</sub> O <sub>29.8</sub>	C <sub>111</sub> H <sub>100</sub> Mn <sub>6</sub> Ca <sub>2</sub> N <sub>9</sub> O <sub>28.5</sub> Cl <sub>4</sub>	C <sub>93.88</sub> H <sub>107.62</sub> Mn <sub>8</sub> CaN <sub>12</sub> O <sub>36.94</sub>	C <sub>93</sub> H <sub>105</sub> Mn <sub>8</sub> Ca <sub>2</sub> N <sub>12</sub> O <sub>36</sub> Cl <sub>27</sub>
FW <sup>a</sup> / g mol <sup>-1</sup>	1721.61	2567.59	2474.64	3443.71
Crystal type	Brown plate	Red rod	Dark-brown plate	Brown plate
Crystal size / mm	0.28×0.49×0.80	0.20×0.04×0.04	0.08×0.07×0.06	0.16×0.16×0.08
Crystal system	Monoclinic	Orthorhombic	Orthorhombic	Monoclinic
Space group	<i>C2/c</i>	<i>Pnna</i>	<i>Pbca</i>	<i>P2<sub>1</sub>/c</i>
<i>a</i> / Å	26.9129(5)	20.4296(8)	19.897(2)	17.0486(7)
<i>b</i> / Å	14.1766(3)	24.9250(10)	21.418(2)	20.8611(8)
<i>c</i> / Å	24.1414(4)	21.6928(8)	47.738(5)	21.1323(8)
<i>α</i> / °	90	90	90	90
<i>β</i> / °	92.403(1)	90	90	111.309(2)
<i>γ</i> / °	90	90	90	90
<i>V</i> / Å <sup>3</sup>	9202.7(3)	11046.1(7)	20344(4)	7001.9(5)
<i>Z</i>	4	4	8	2
<i>T</i> / K	293	100.0(2)	100.0(2)	150(2)
<i>ρ</i> <sub>calc</sub> / g cm <sup>-3</sup>	1.243	1.544	1.616	1.633
<i>μ</i> / mm <sup>-1</sup>	5.951	1.705	1.388	1.359
<i>θ</i> range / °	6.60 - 64.99	2.34 - 39.33	2.63 - 29.42	3.65 - 25.03

Index ranges	$-31 \leq h \leq 31$	$-29 \leq h \leq 29$	$-25 \leq h \leq 25$	$-20 \leq h \leq 20$
	$-13 \leq k \leq 16$	$-35 \leq k \leq 35$	$-26 \leq k \leq 27$	$-24 \leq k \leq 24$
	$-28 \leq l \leq 28$	$-31 \leq l \leq 31$	$-60 \leq l \leq 60$	$-25 \leq l \leq 25$
Collected reflections	44128	245372	171165	88540
Independent reflections	7680 ( $R_{\text{int}} = 0.0732$ )	16916 ( $R_{\text{int}} = 0.0507$ )	21624 ( $R_{\text{int}} = 0.0928$ )	7805 ( $R_{\text{int}} = 0.0831$ )
Final $R^{b,c}$ indices [ $I > 2\sigma(I)$ ]	$R1 = 0.0711^d$ $wR2 = 0.2008^d$	$R1 = 0.0735$ $wR2 = 0.1932$	$R1 = 0.0547$ $wR2 = 0.1321$	$R1 = 0.1351$ $wR2 = 0.3940$
$(\Delta\rho)_{\text{max,min}} / \text{e } \text{\AA}^{-3}$	0.668, -0.513	1.427, -1.363	0.977, -0.562	5.790, -1.591

<sup>a</sup>Including solvate molecules. <sup>b</sup> $R1 = \Sigma(|F_o| - |F_c|)/\Sigma|F_o|$ . <sup>c</sup> $wR2 = [\Sigma[w(F_o^2 - F_c^2)^2]/\Sigma[w(F_o^2)^2]]^{1/2}$ ,  $w = 1/[\sigma^2(F_o^2) + (ap)^2 + bp]$ , where  $p = [\max(F_o^2, 0) + 2F_c^2]/3$ . <sup>d</sup>For 5879 reflections with  $I > 2\sigma(I)$ .

**Physical Measurements.** Infrared (IR) spectra were recorded in the solid state on a Bruker's FT-IR spectrometer (ALPHA's Platinum ATR single reflection) in the 4000-400  $\text{cm}^{-1}$  range. Elemental analyses (C, H, and N) were performed on a Perkin-Elmer 2400 Series II Analyzer. Magnetic susceptibility studies were performed at the Chemistry Department of the University of Florida on a Quantum Design MPMS-XL SQUID susceptometer equipped with a 7 T magnet and operating in the 1.8-400 K range. Samples were embedded in solid eicosane to prevent torquing. Pascal's constants were used to estimate the diamagnetic correction, which was subtracted from the experimental susceptibility to give the molar paramagnetic susceptibility ( $\chi_M$ ).<sup>42</sup>

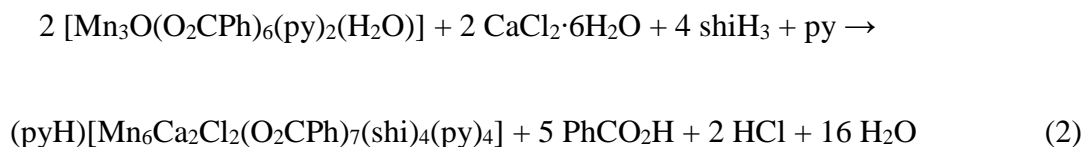
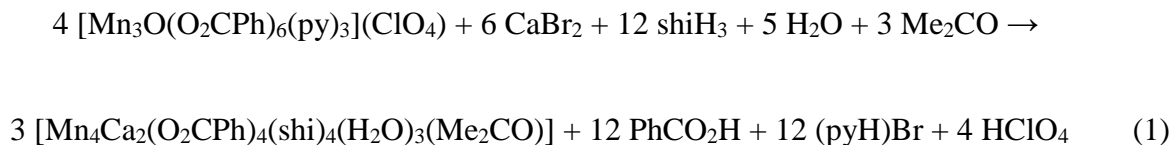
## RESULTS AND DISCUSSION



**Synthesis and IR Spectra.** Two different synthetic strategies were employed for the synthesis and crystallization of the reported heterometallic Mn-Ca cluster compounds. The first utilizes either the charged  $[\text{Mn}_3\text{O}(\text{O}_2\text{CPh})_6(\text{py})_3]^+$  triangle as starting material, which comprises 3  $\text{Mn}^{\text{III}}$  atoms, or the mixed-valence, neutral  $[\text{Mn}_3\text{O}(\text{O}_2\text{CPh})_6(\text{py})_2(\text{H}_2\text{O})]$  triangle ( $2\text{Mn}^{\text{III}}, 1\text{Mn}^{\text{II}}$ ), in the presence of  $\text{CaX}_2$  sources ( $\text{X}^- = \text{halides}$ ; Br (for **1**) and Cl (for **2**)) and salicylhydroxamic acid ( $\text{shaH}_2$ ). In this first route, no external organic base was used as the role of proton acceptor could be undertaken by the carboxylate groups, pyridine molecules and/or oxido ions of the  $\{\text{Mn}_3\}$  starting materials. The oxide-centered and carboxylate-bridged  $\{\text{Mn}_3\}$  triangles have been proven to be invaluable sources for the synthesis of high-nuclearity, homometallic  $\{\text{Mn}_x\}$  clusters of various large nuclearities and high oxidation states for the metal atoms.<sup>43</sup> The second route that was followed includes the reactions between simpler, monomeric  $\text{Mn}^{\text{II}}$ - and  $\text{Ca}^{\text{II}}$ -containing starting materials in the presence of the chelating/bridging organic ligand  $\text{shaH}_2$  and base  $\text{NEt}_3$ . The latter was used to facilitate the deprotonation of the  $\text{shaH}_2/\text{shiH}_3$  ligands and subsequently generate  $\text{NHEt}_3^+$  cations in solution, which can potentially counterbalance the anionic charge of a cluster compound in solution and help with the crystallization of the resulting salt in the solid-state. Finally, various solvents and metals: $\text{shaH}_2$  ratios were explored to target for the crystallization of the reported molecular compounds.

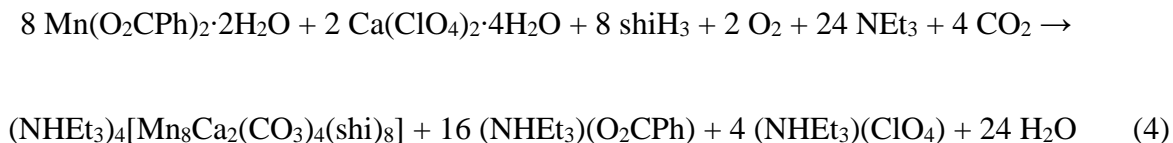
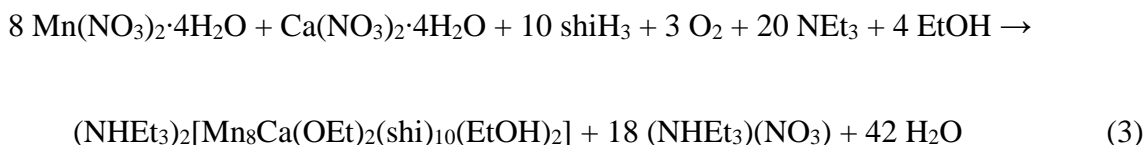
Therefore, the one-pot reaction of  $[\text{Mn}_3\text{O}(\text{O}_2\text{CPh})_6(\text{py})_3](\text{ClO}_4)$  and  $\text{CaBr}_2 \cdot x\text{H}_2\text{O}$  with  $\text{shaH}_2$  in a 1:1.5:3 molar ratio in  $\text{Me}_2\text{CO}$  gave a dark brown solution that, upon filtration and slow evaporation at room temperature, afforded brown crystals of the complex  $[\text{Mn}^{\text{III}}_4\text{Ca}_2(\text{O}_2\text{CPh})_4(\text{shi})_4(\text{H}_2\text{O})_3(\text{Me}_2\text{CO})]$  (**1**) in 60% yield (based on the total available Ca). A similar reaction with that of **1**, albeit with  $[\text{Mn}_3\text{O}(\text{O}_2\text{CPh})_6(\text{py})_2(\text{H}_2\text{O})]$  and  $\text{CaCl}_2 \cdot 6\text{H}_2\text{O}$  in the presence of  $\text{shaH}_2$ , in a molar ratio of 1:1:1 and in solvent  $\text{CH}_2\text{Cl}_2$ , led to a brown solution that,

upon filtration and slow diffusion with Et<sub>2</sub>O, afforded red crystals of a new, mixed-valence complex (pyH)[Mn<sup>II</sup><sub>2</sub>Mn<sup>III</sup><sub>4</sub>Ca<sub>2</sub>Cl<sub>2</sub>(O<sub>2</sub>CPh)<sub>7</sub>(shi)<sub>4</sub>(py)<sub>4</sub>] (**2**) in 45% yield (based on the total available Ca). The formation of complexes **1** and **2** is summarized in the balanced eqs 1 and 2, respectively.



Analogous reactions with different carboxylate-based {Mn<sub>3</sub>} triangles as starting materials (i.e., acetates, propionates, pivalates, etc.), all failed to yield single-crystals suitable for X-ray diffraction studies. We have thus turned our synthetic endeavors towards one-pot reactions between Mn(NO<sub>3</sub>)<sub>2</sub>·4H<sub>2</sub>O, Ca(NO<sub>3</sub>)<sub>2</sub>·4H<sub>2</sub>O, shaH<sub>2</sub> and NEt<sub>3</sub> in various molar ratios and solvents. Only from the 1:1:1:3 reaction of the aforementioned precursors in solvent EtOH we were able to grow dark-brown crystals of a nonanuclear, mixed-valence complex (NHEt<sub>3</sub>)<sub>2</sub>[Mn<sup>III</sup><sub>4</sub>Mn<sup>IV</sup><sub>4</sub>Ca(OEt)<sub>2</sub>(shi)<sub>10</sub>(EtOH)<sub>2</sub>] (**3**) in 30% yield (based on the total available Ca). It becomes apparent that the reaction solvent has an important role in the synthesis and crystallization of **3**; both bridging EtO<sup>-</sup> groups and terminally-bound EtOH molecules were

found in the structure of **3** (*vide infra*). Reactions in different alcohols did not yield any crystalline materials but only amorphous precipitates that we were unable to re-dissolve and crystallize. Expanding this synthetic protocol further, we decided to perform the 1:1:1:3 reaction between  $\text{Mn}(\text{O}_2\text{CPh})_2 \cdot 2\text{H}_2\text{O}$ ,  $\text{Ca}(\text{ClO}_4)_2 \cdot 4\text{H}_2\text{O}$ ,  $\text{shiH}_2$  and  $\text{NEt}_3$  in solvent  $\text{CHCl}_3$ . The resulting brown solution was left to evaporate slowly at room temperature and, over a period of approximately one month, brown crystals formed in yields as high as 20%, which turned out to be a new decanuclear complex  $(\text{NHEt}_3)_4[\text{Mn}^{\text{III}}_8\text{Ca}_2(\text{CO}_3)_4(\text{shi})_8]$  (**4**). The coordinated  $\text{CO}_3^{2-}$  ions (*vide infra*) were presumably derived from the fixation of atmospheric  $\text{CO}_2$  during aerobic reactions.<sup>44</sup> This could also explain the prolonged crystallization period of **4** when compared to the other compounds **1-3**. The formation of complexes **3** and **4** is summarized in the balanced eqs 3 and 4, respectively.



The reactions that gave **3** and **4** are both oxidations, undoubtedly by  $\text{O}_2$  under the prevailing basic conditions. None of the anions accompanying the metal ions' starting materials appear to

participate in the molecular structures of **3** and **4**. The NEt<sub>3</sub> has the role of proton acceptor to facilitate the deprotonation of the shiH<sub>3</sub> groups and solvate molecules (i.e., EtOH to EtO<sup>-</sup>). In addition, both anionic clusters **3** and **4** are stabilized by NHEt<sub>3</sub><sup>+</sup> counterocations. Employment of different organic bases, such as NMe<sub>3</sub>, Bu<sup>n</sup><sub>3</sub>N and Me<sub>4</sub>NOH, did not afford crystalline materials but only oily products that we were not able to further characterize. In all complexes **1-4**, the coordinated shi<sup>3-</sup> groups resulted from the metal ion-assisted transformation of shaH<sub>2</sub> under the reported synthetic conditions (*vide infra*). Finally, by adjusting the experimental molar ratios of the precursors to the stoichiometric equivalents, in an attempt to optimize the isolated yields, we failed to reproduce the crystals of all reported complexes.

Unfortunately, complexes **1-4** do not appear to retain their solid-state structures in solutions of various solvent media (i.e., MeCN, CH<sub>2</sub>Cl<sub>2</sub> and THF), as it was confirmed by electrospray ionization mass spectrometry (ESI-MS). It is very possible that this diversity of species in solution is one of the main reasons for crystallizing and structurally characterizing in the solid-state four different compounds from the Mn-Ca/shaH<sub>2</sub> reaction system. We have thus concentrated on the solid-state characterization of these species, which includes IR spectroscopy and magnetic susceptibility studies. All complexes **1-4** have similar IR spectra which are dominated by the stretching vibrations of the aromatic rings of shi<sup>3-</sup> in the ~1595-1380 cm<sup>-1</sup> range; these bands in complexes **1** and **2** overlap with stretches from the carboxylate groups, thus rendering their exact assignments very difficult.<sup>45</sup> Contributions from the  $\nu(\text{C}=\text{N})_{\text{oximate}}$  modes of shi<sup>3-</sup> would be also expected in this region. It is very likely that the strong bands at 1595/1432 cm<sup>-1</sup> and 1597/1432 cm<sup>-1</sup> in the spectra of **1** and **2** are attributed to the  $\nu_{\text{as}}(\text{CO}_2)$  and  $\nu_{\text{s}}(\text{CO}_2)$  modes, respectively; the former should also involve a ring stretching character. The difference  $\Delta$  [ $\Delta = \nu_{\text{as}}(\text{CO}_2) - \nu_{\text{s}}(\text{CO}_2)$ ] is small (<165 cm<sup>-1</sup>) in both cases, as expected for the predominant

bidentate bridging mode of carboxylate ligation (*vide infra*).<sup>26,46</sup> The bands at ~3060, ~2990 and ~2970 cm<sup>-1</sup> in complexes **1**, **3** and **4** can be assigned to the stretching vibrations of  $\nu(\text{N-H})$  modes from the presence of  $\text{NHEt}_3^+$  counteranions.<sup>26,47</sup> Finally, the carbonate-related IR bands in **4** could be tentatively assigned to the bands located at ~1448 and 863 cm<sup>-1</sup>, as previously observed in other carbonate-bridged metal complexes.<sup>48</sup>

**Description of Structures.** The Mn oxidation states in all complexes **1-4** were established by charge balance considerations, metric parameters and bond valence sum calculations (BVS,<sup>49</sup> Table 2). Selected interatomic distances and angles for complexes **1-4** are listed in Tables S1-S4, respectively. The crystal structure of **1** consists of  $[\text{Mn}_4\text{Ca}_2(\text{O}_2\text{CPh})_4(\text{shi})_4(\text{H}_2\text{O})_3(\text{Me}_2\text{CO})]$  molecules (Figure 1, top) and lattice  $\text{Me}_2\text{CO}$  and  $\text{H}_2\text{O}$  solvate molecules; the latter two will not be further discussed.

The centrosymmetric core of **1** comprises four  $\text{Mn}^{\text{III}}$  and two  $\text{Ca}^{\text{II}}$  atoms arranged in a slightly distorted octahedral topology (Figure 1, bottom right), with the  $\text{Ca}^{\text{II}}$  atoms occupying the apical positions and the  $\text{Mn}^{\text{III}}$  atoms forming the square base. The  $\text{Mn}\cdots\text{Mn}\cdots\text{Mn}$  angles are 89.7 and 90.3°, deviating only slightly from the ideal 90°, and the  $\text{Mn}\cdots\text{Ca}\cdots\text{Mn}$  angles of the eight triangular faces lie within the 75.6-77.5° range. The  $\text{Mn}^{\text{III}}$  atoms form a near-planar square, with each of the edges bridged by a diatomic oximate group from a  $\text{shi}^{3-}$  ligand, thus giving  $\text{Mn}\cdots\text{Mn}$  separations of 4.623(1) and 4.652(1) Å. The almost perfectly planar  $\text{Mn}_4$  unit is clearly due to the large Mn-O-N-Mn torsion angles of 176.7 and 177.6° for the Mn1-O2-N1-Mn2 and Mn2-O12'-N11'-Mn1' units (and their symmetry-related counterparts), respectively, very close to the ideal linearity of 180°. The  $\text{Ca}^{\text{II}}$  atoms are displaced by 1.784 Å out of the  $\text{Mn}_4$  best-mean-plane. The linkage between the basal  $\text{Mn}^{\text{III}}$  atoms and the apical  $\text{Ca}^{\text{II}}$  atoms is provided by the oximate O

atoms (O2, O2', O12 and O12') of shi<sup>3-</sup> ligands and the four  $\eta^1:\eta^1:\mu$  bidentate bridging benzoate groups; the latter are in pairs of two above and below the Mn<sub>4</sub> basal plane.

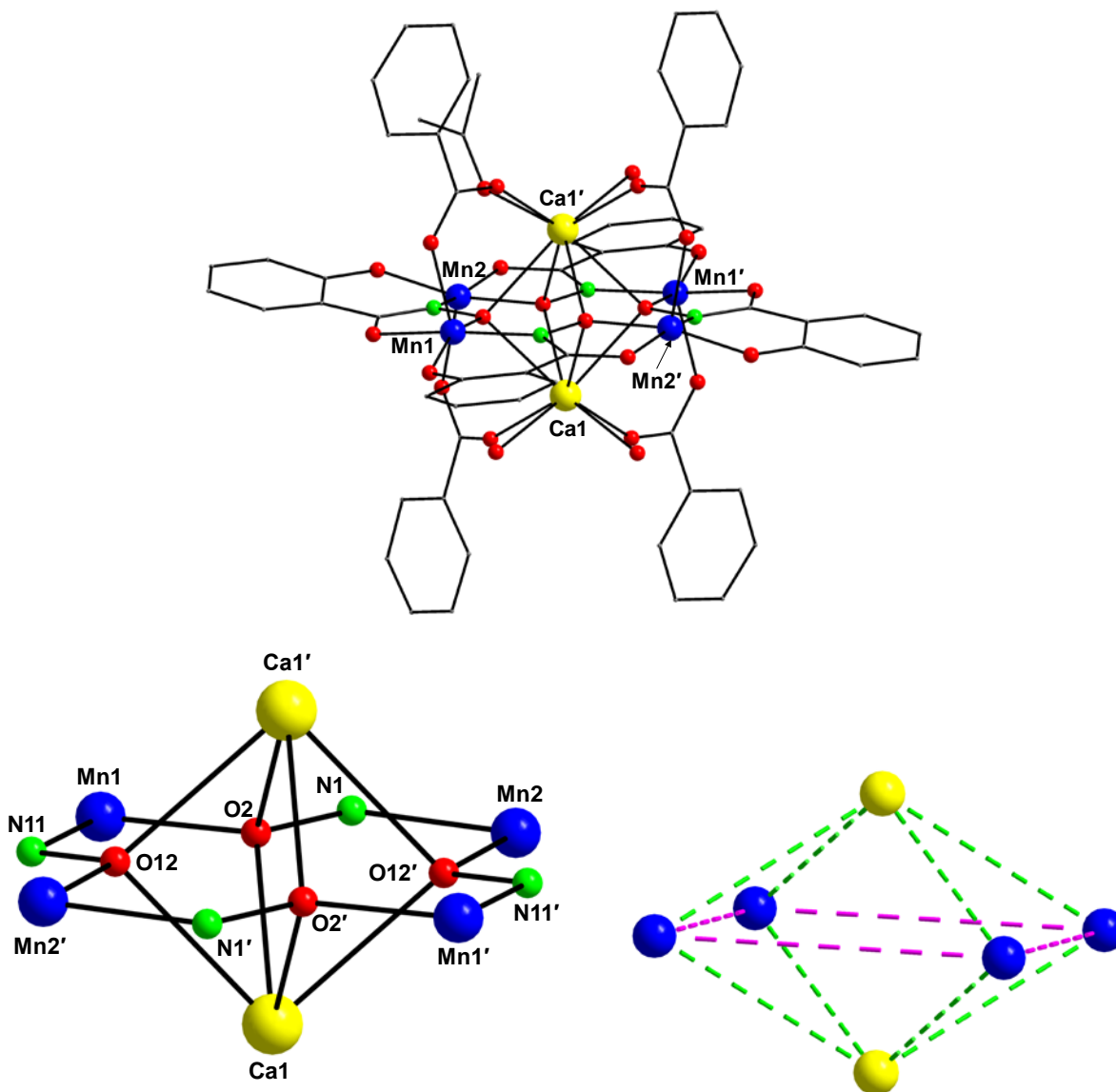


**Figure 1.** Partially labeled representations of the structure of **1** (top), its complete  $[\text{Mn}_4\text{Ca}_2(\mu_3\text{-NO})_4]^{12+}$  core (bottom, left) and the  $\{\text{Mn}_4\text{Ca}_2\}$  octahedral topology (bottom, right). The green and purple dashed lines represent virtual  $\text{Mn}\cdots\text{Ca}$  and  $\text{Mn}\cdots\text{Mn}$  bonds. Color scheme:  $\text{Mn}^{\text{III}}$  blue,  $\text{Ca}^{\text{II}}$  yellow, O red, N green, C gray. H atoms are omitted for clarity. Symmetry operation for the primed atoms in **1**:  $0.5-x, 0.5-y, -z$ .

Ligation around each Mn<sup>III</sup> atom is completed by the alkoxido and phenoxido O atoms from the shi<sup>3-</sup> groups; the latter are thus  $\eta^1:\eta^1:\eta^1:\eta^3:\mu_4$  (Scheme 3). The complex therefore contains an overall [Mn<sub>4</sub>Ca<sub>2</sub>( $\mu_3$ -NO)<sub>4</sub>]<sup>12+</sup> core (Figure 1, bottom left) which can also be described as a [12-MC<sub>Mn(III)N(shi)-4</sub>] metallocrown<sup>50</sup> with two Ca<sup>II</sup> atoms displaced out of the arrangement. All Ca-O bonds are in the range 2.264(3)-2.595(3) Å. All Mn<sup>III</sup> atoms in **1** are five-coordinate with almost perfect square pyramidal geometries. This was confirmed by analysis of the shape-determining bond angles using the approach of Reedijk and Addison,<sup>51</sup> which yields an average value for the trigonality index,  $\tau$ , of 0.05 for the four metal ions, where  $\tau$  is 0 and 1 for perfect square pyramidal and trigonal bipyramidal geometries, respectively. The Ca<sup>II</sup> atoms are eight-coordinate in a CaO<sub>8</sub> environment possessing square antiprismatic geometries. That was confirmed by the Continuous Shape Measure (CShM) approach which essentially allows one to numerically evaluate by how much a particular geometry deviates from an ideal shape.<sup>52</sup> The best fit was obtained for the square antiprism (Figure S1) with a CShM value of 2.21. Values of CShM between 0.1 and 3 usually correspond to a non-negligible but still small distortion from ideal geometry.<sup>53</sup>

The coordination spheres of the Ca<sup>II</sup> atoms in **1** are completed by three and one terminally bound water and acetone molecules, respectively. Recall that four coordinated H<sub>2</sub>O molecules were found in the active site of the native OEC, two of which are bound to the Ca<sup>II</sup> atom. These water molecules could serve as substrates for the overall catalytic reaction to proceed, including subsequent deprotonations with metal-centered oxidations preceding O-O bond formation.<sup>54</sup> To that end, complex **1** may be of some interest to the catalytic cycle of the OEC.

**Scheme 3. Coordination Modes of All Bridging Ligands in Complexes 1-4**

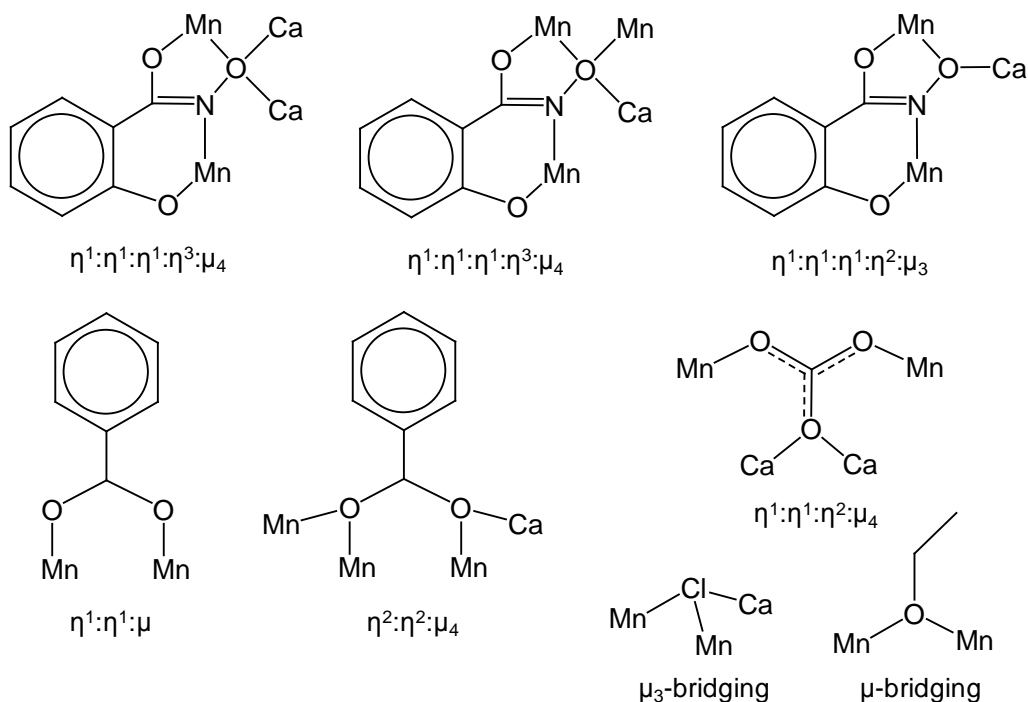


**Table 2. BVS Calculations<sup>a</sup> for Mn Atoms in Complexes 1-4**

Complex	Atom	Mn <sup>II</sup>	Mn <sup>III</sup>	Mn <sup>IV</sup>
<b>1</b>	Mn1	3.30	<u>3.05</u>	3.14
	Mn2	3.21	<u>2.97</u>	3.06
<b>2</b>	Mn1	<u>2.01</u>	1.65	1.68
	Mn2	3.21	<u>2.98</u>	3.06
	Mn3	3.20	<u>2.97</u>	3.05
<b>3</b>	Mn1	3.36	<u>3.11</u>	3.21
	Mn2	3.37	<u>3.12</u>	3.22
	Mn3	4.44	4.14	<u>4.22</u>
	Mn4	4.30	3.98	<u>4.10</u>
	Mn5	4.41	4.11	<u>4.19</u>
	Mn6	3.13	<u>2.90</u>	2.98
	Mn7	3.33	<u>3.09</u>	3.18
	Mn8	4.39	4.06	<u>4.19</u>



<b>4</b>	Mn1	3.37	<u>3.12</u>	3.21
	Mn2	3.36	<u>3.11</u>	3.20
	Mn3	3.34	<u>3.09</u>	3.18
	Mn4	3.36	<u>3.11</u>	3.20

<sup>a</sup> The underlined value is the one closest to the charge for which it was calculated. The oxidation state is the nearest whole number to the underlined value.

The crystal structure of **2** consists of  $[\text{Mn}_6\text{Ca}_2\text{Cl}_2(\text{O}_2\text{CPh})_7(\text{shi})_4(\text{py})_4]^-$  anions (Figure 2, top) counterbalanced by  $\text{pyH}^+$  cations. In addition, there are  $\text{CH}_2\text{Cl}_2$  and  $\text{Et}_2\text{O}$  solvate molecules in the crystal lattice, which will not be further discussed. The structure of the anion of **2** comprises a  $\{\text{Mn}^{\text{III}}_4\text{Ca}_2\}$  octahedron, reminiscent to the discrete structure of complex **1**, linked to an additional  $\{\text{Mn}^{\text{II}}_2\}$  dimer through two bridging  $\text{Cl}^-$  ions and two  $\eta^2:\eta^2:\mu_4$   $\text{PhCO}_2^-$  groups (Scheme 3). The  $\text{Mn}\cdots\text{Mn}\cdots\text{Mn}$  angles within the  $\{\text{Mn}^{\text{III}}_4\text{Ca}_2\}$  octahedron are  $89.6$  and  $90.4^\circ$ , again deviating only slightly from the ideal  $90^\circ$ , and the  $\text{Mn}\cdots\text{Ca}\cdots\text{Mn}$  angles of the eight triangular faces lie within the  $74.5$ - $79.0^\circ$  range. The two  $\text{Ca}^{\text{II}}$  atoms lie  $1.990$  Å (Ca1) and  $1.582$  Å (Ca2) out of the  $\text{Mn}_4$  square plane. Similar to complex **1**, the linkage between the basal  $\text{Mn}^{\text{III}}$  atoms and the apical  $\text{Ca}^{\text{II}}$  atoms is provided by the oximate O atoms (O1, O1', O4 and O4') of  $\text{shi}^{3-}$  ligands and four  $\eta^1:\eta^1:\mu$  bidentate bridging benzoate groups, which are all pointed towards Ca1. The two  $\text{Mn}^{\text{II}}$  atoms, which are located below Ca2, are further bridged to each other through an  $\eta^1:\eta^1:\mu$   $\text{PhCO}_2^-$  group, while their coordination spheres are completed by four terminally bound pyridine molecules. The  $\text{Mn}^{\text{II}}\cdots\text{Mn}^{\text{II}}$  distance is  $3.400(1)$  Å. The overall metal topology of **2** (Figure 2, bottom right) and its  $[\text{Mn}^{\text{II}}_2\text{Mn}^{\text{III}}_4\text{Ca}_2(\mu_3\text{-Cl})_2(\mu_4\text{-O}_2\text{CPh})_2(\mu_4\text{-NO})_4]^{12+}$  core (Figure 2, bottom left) are finally stabilized by the coordinated alkoxido and phenoxido O atoms from the  $\eta^1:\eta^1:\eta^1:\eta^3:\mu_4$   $\text{shi}^{3-}$  groups.

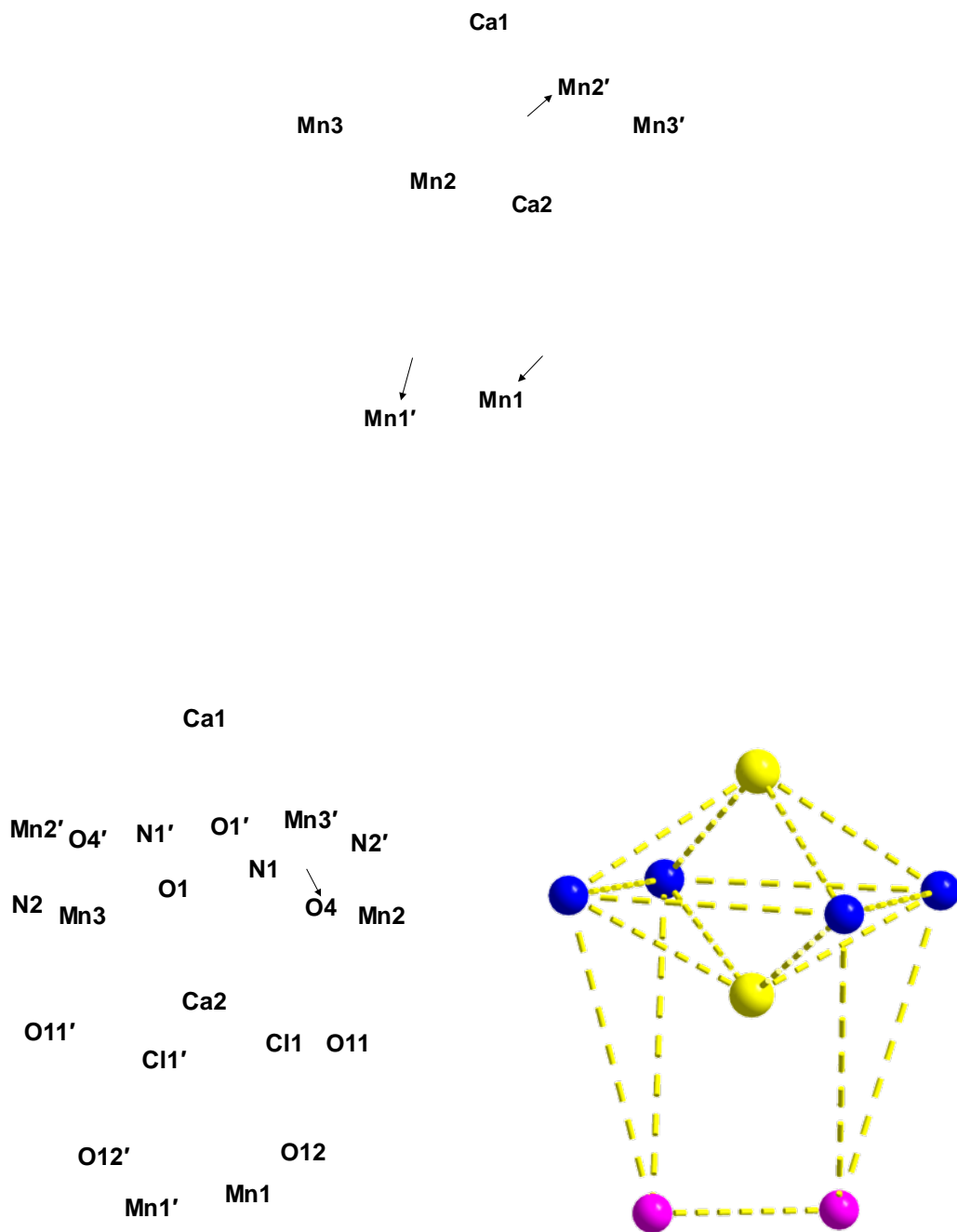


**Figure 2.** Partially labeled representations of the anion of complex **2** (top), its complete  $[\text{Mn}^{\text{II}}_2\text{Mn}^{\text{III}}_4\text{Ca}_2(\mu_3\text{-Cl})_2(\mu_4\text{-O}_2\text{CPh})_2(\mu_3\text{-NO})_4]^{12+}$  core (bottom, left) and the  $\{\text{Mn}_6\text{Ca}_2\}$  topology

(bottom, right). The yellow dashed lines represent virtual Mn $\cdots$ Ca and Mn $\cdots$ Mn bonds. Color scheme: Mn<sup>II</sup> purple, Mn<sup>III</sup> blue, Ca<sup>II</sup> yellow, O red, N green, Cl cyan, C gray. H atoms are omitted for clarity. Symmetry operation for the primed atoms in **2**:  $x, 0.5-y, 1.5-z$ .

All Mn atoms in **2** are six-coordinate with distorted octahedral geometries. In the case of the Mn<sup>III</sup> atoms (Mn2, Mn2', Mn3 and Mn3'), the octahedra take the form of axially elongated Jahn-Teller (JT) distortions, as expected for high-spin d<sup>4</sup> ions in this geometry. The JT axes in all Mn<sup>III</sup> sites involve the carboxylate O atoms and the Cl<sup>-</sup> groups. In addition, both Ca<sup>II</sup> atoms in **2** are eight-coordinate albeit with different coordination geometries, as established by Continuous Shape Measures (CShM). The best fit was obtained for the square antiprism (Ca1) and biaugmented trigonal prism (Ca2) with CShM values of 1.19 and 3.98, respectively (Figure S2). Given the presence of Cl<sup>-</sup> groups in the vicinity of the active site of the native OEC and their structural role in both maintaining the coordination environment of the {Mn<sub>4</sub>Ca} cluster and functioning as either proton exit channels or water inlet channels,<sup>13</sup> complex **2** could be structurally interesting as it is only -to the best of our knowledge- the second Cl-bridged Mn-Ca cluster reported to date (Table 3).

The crystal structure of **3** consists of [Mn<sub>8</sub>Ca(OEt)<sub>2</sub>(shi)<sub>10</sub>(EtOH)<sub>2</sub>]<sup>2-</sup> dianions (Figure 3, top), each of which is counterbalanced by two NH<sub>4</sub><sup>+</sup> cations. In addition, there are EtOH and H<sub>2</sub>O solvate molecules in the crystal lattice, which will not be further discussed. The asymmetric dianion of **3** comprises four Mn<sup>III</sup> (Mn1, Mn2, Mn6 and Mn7) and four Mn<sup>IV</sup> (Mn3, Mn4, Mn5 and Mn8) atoms (Table 2), bridged together through the oximate groups of eight  $\eta^1:\eta^1:\eta^1:\eta^2:\mu_3$ - and two  $\eta^1:\eta^1:\eta^1:\eta^3:\mu_4$  shi<sup>3-</sup> groups (Scheme 3). Furthermore, there are also two EtO<sup>-</sup> groups

bridging two different pairs of Mn<sup>III</sup> atoms (Mn1/Mn6 and Mn2/Mn7). The eight Mn atoms are arranged in a very distorted ring-like topology with the four Mn<sup>III</sup> and Mn<sup>IV</sup> atoms being on opposite sides and the oximate O atoms serving to link the Mn<sub>8</sub> 'ring' with the central Ca<sup>II</sup> atom. As a result, the Ca<sup>II</sup> atom is surrounded by ten O atoms and possesses a coordination geometry that can be described as sphenocorona (CShM = 2.84; Figure S3). All Mn atoms are six-coordinate with near-octahedral geometries, while the axially elongated Mn<sup>III</sup> octahedra are JT-distorted with oximate and alkoxido O atoms occupying the four JT axes.

Complex **3** has an overall [Mn<sup>III</sup><sub>4</sub>Mn<sup>IV</sup><sub>4</sub>Ca(μ-OEt)<sub>2</sub>(μ<sub>4</sub>-NO)<sub>2</sub>(μ<sub>3</sub>-NO)<sub>8</sub>]<sup>18+</sup> core (Figure 3, bottom). The Mn⋯Mn and Mn⋯Ca distances span the range 3.283(1)-7.599(1) Å and 3.545(1)-4.048(1) Å, respectively, whereas the Mn-O-N-Mn torsion angles lie within the 96.9-174.7° range. The smallest torsion angles (~97-99°) are between the Mn<sup>III</sup>⋯Mn<sup>III</sup> pairs and they deviate significantly from linearity. This is most likely the main reason for the stabilization of the asymmetric structure of **3**, and consequently for a first time in Mn-Ca/shi<sup>3-</sup> chemistry we observed a structural motif that does not contain any discrete or repeating {Mn<sub>4</sub>Ca} square pyramidal units. Finally, complex **3** is a rare example of a heterometallic Mn-Ca cluster containing both Mn<sup>III</sup> and Mn<sup>IV</sup> atoms, and the first non-oxido bridged complex with an unprecedented 8:1 Mn-to-Ca metal ratio (Table 3).

Mn8 Mn4  
 Mn3 Mn5  
 Ca1  
 Mn7 Mn1  
 Mn2 Mn6

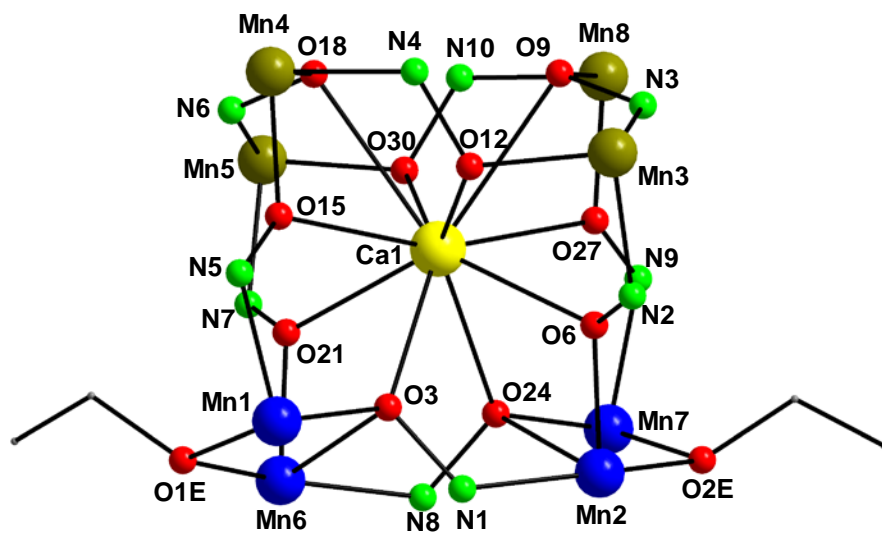


**Figure 3.** Partially labeled representations of the dianion of complex **3** (top), and its complete  $[\text{Mn}^{\text{III}}_4\text{Mn}^{\text{IV}}_4\text{Ca}(\mu\text{-OEt})_2(\mu_4\text{-NO})_2(\mu_3\text{-NO})_8]^{18+}$  core (bottom). Color scheme:  $\text{Mn}^{\text{III}}$  blue,  $\text{Mn}^{\text{IV}}$  olive green,  $\text{Ca}^{\text{II}}$  yellow, O red, N green, C gray. H atoms are omitted for clarity.

The crystal structure of **4** consists of  $[\text{Mn}_8\text{Ca}_2(\text{CO}_3)_4(\text{shi})_8]^{4-}$  tetraanions (Figure 4, top), each of which is counterbalanced by four  $\text{NHET}_3^+$  cations. The latter cations are hydrogen-bonded with the coordinated carbonato O atoms. In addition, there are  $\text{CHCl}_3$  solvate molecules in the crystal lattice, which will not be further discussed. The centrosymmetric complex  $[\text{Mn}_8\text{Ca}_2(\text{CO}_3)_4(\text{shi})_8]^{4-}$  is arranged as two parallel  $\{\text{Mn}_4\text{Ca}\}$  square pyramids that are linked to each other through four  $\eta^1:\eta^1:\eta^2:\mu_4 \text{CO}_3^{2-}$  groups (Scheme 3). The two  $\text{Ca}^{\text{II}}$  atoms are both pointed towards the center of a cavity that is formed by the rectangular cuboidal (or rectangular parallelepiped) arrangement of the eight external  $\text{Mn}^{\text{III}}$  atoms (Figure 4, bottom right). As a result, the  $\{\text{Mn}_8\text{Ca}_2\}$  compound possesses a virtual  $D_{2h}$  point group. The opposite faces of the rectangular cuboid comprise the atoms  $\text{Mn}(1,2,3,4)/\text{Mn}(1',2',3',4')$  and  $\text{Mn}(1,3,2',4')/\text{Mn}(1',3',2,4)$  with  $\text{Mn}\cdots\text{Mn}$  distances spanning the range 4.612(3)-4.638(1) Å and 4.623(2)-6.122(3) Å, respectively. The  $\text{Mn}\cdots\text{Mn}\cdots\text{Mn}$  angles lie within the 89.7-90.1° range, very close to the ideal 90° for a perfect rectangular cuboid. The linkage between the basal  $\text{Mn}^{\text{III}}$  atoms and the apical  $\text{Ca}^{\text{II}}$  atoms within each  $\{\text{Mn}_4\text{Ca}\}$  square pyramid is provided by the oximate O atoms (O1, O7, O6, O18 and their symmetry-related partners) of eight  $\text{shi}^{3-}$  ligands; the latter are thus  $\eta^1:\eta^1:\eta^1:\eta^2:\mu_3$  (Scheme 3). The four basal  $\text{Mn}^{\text{III}}$  atoms form a near-planar square, with each of the edges bridged by a diatomic oximate group from a  $\text{shi}^{3-}$  ligand. The almost perfectly planar  $\text{Mn}_4$  units are clearly due to the large Mn-O-N-Mn torsion angles of  $\sim 179^\circ$ , very close to the ideal linearity of  $180^\circ$ . The linkage between the Mn atoms of the two  $\{\text{Mn}_4\text{Ca}\}$  square

pyramids is provided by the *anti-anti* O atoms of the four bridging  $\text{CO}_3^{2-}$  groups (Scheme 3). Ca1 and Ca1' lie 1.556 Å below and above the corresponding  $\text{Mn}_4$  best-mean-planes, respectively.

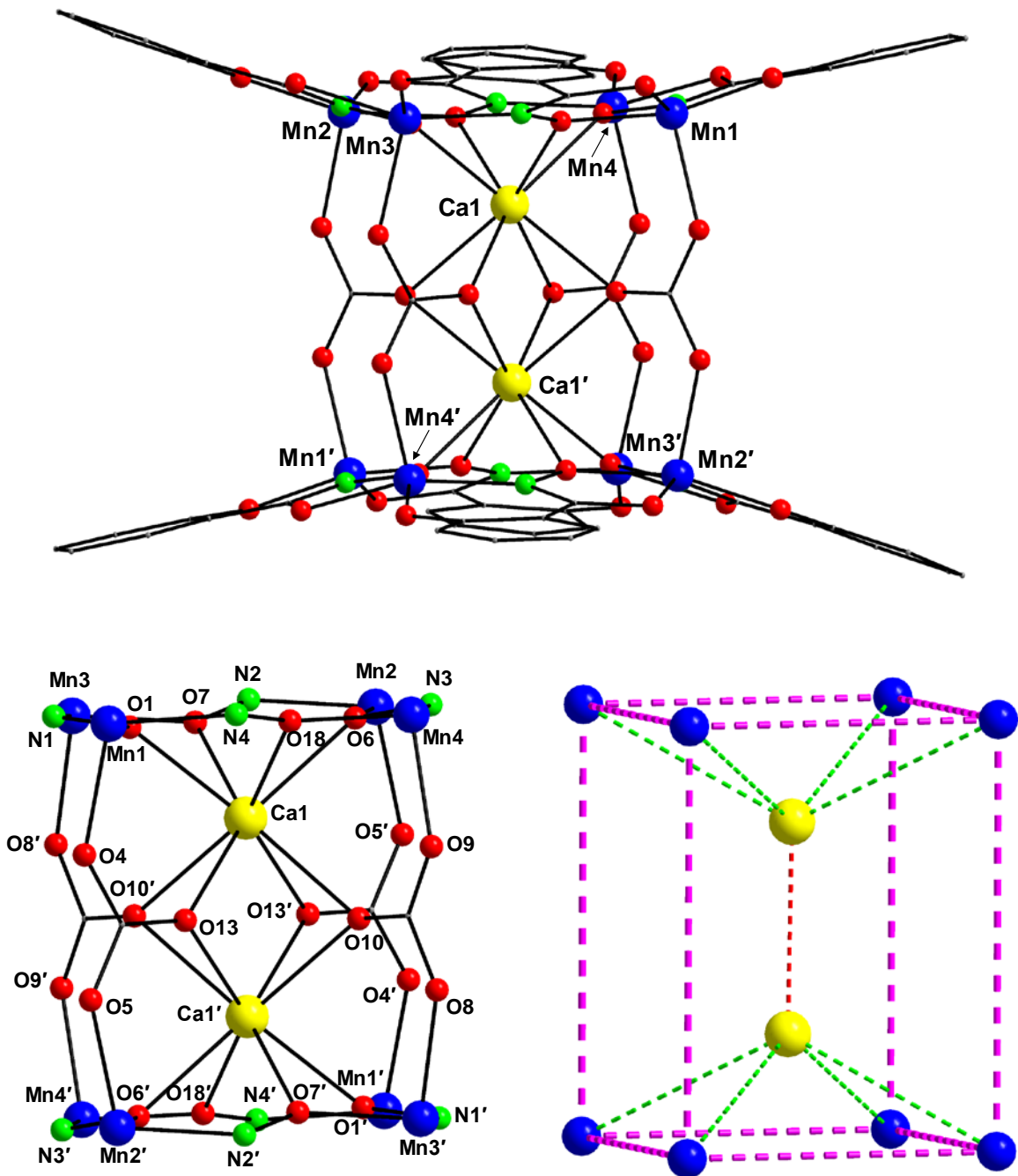


**Figure 4.** Partially labeled representations of the tetraanion of complex **4** (top), its complete  $[\text{Mn}_8\text{Ca}_2(\mu_4\text{-CO}_3)_4(\mu_3\text{-NO})_8]^{12+}$  core (bottom, left) and the  $\{\text{Mn}_8\text{Ca}_2\}$  rectangular cuboidal topology (bottom, right). The green, purple and red dashed lines represent virtual  $\text{Mn}\cdots\text{Ca}$ ,  $\text{Mn}\cdots\text{Mn}$  and  $\text{Ca}\cdots\text{Ca}$  bonds. Color scheme:  $\text{Mn}^{\text{III}}$  blue,  $\text{Ca}^{\text{II}}$  yellow, O red, N green, C gray. H atoms are omitted for clarity. Symmetry operation for the primed atoms in **4**:  $-x, -y, -z$ .

The complex therefore contains an overall  $[\text{Mn}_8\text{Ca}_2(\mu_4\text{-CO}_3)_4(\mu_3\text{-NO})_8]^{12+}$  core (Figure 4, bottom left) which can also be described as two carbonato-bridged  $[12\text{-MCMn(III)N(Shi)-4}]$  metallacrown units surrounding two  $\text{Ca}^{\text{II}}$  atoms. Alternatively, complex **4** can be also seen as a  $\{\text{Mn}_8\}$  molecular ‘capsule’ that accommodates two  $\text{Ca}^{\text{II}}$  atoms in its cavity (Figure 5). To the current degree of knowledge, a more possible scenario is that two solution-stable  $\{\text{Mn}_4\text{Ca}\}$  units were assembled and linked together through the  $\text{CO}_3^{2-}$  groups rather than the two  $\text{Ca}^{\text{II}}$  atoms templating the formation of the outer  $\{\text{Mn}_8\}$  unit. All  $\text{Mn}^{\text{III}}$  atoms in **4** are five-coordinate with almost perfect square pyramidal geometries ( $\tau = 0.07\text{-}0.09$ ). Both  $\text{Ca}^{\text{II}}$  atoms are eight-coordinate in  $\text{CaO}_8$  environments possessing square antiprismatic geometries with a CShM value of 1.86 (Figure S4). Finally, complex **4** is the first heterometallic Mn-Ca complex bearing coordinated carbonato groups and the first Mn-Ca complex with an 8:2 metal stoichiometry (Table 3).



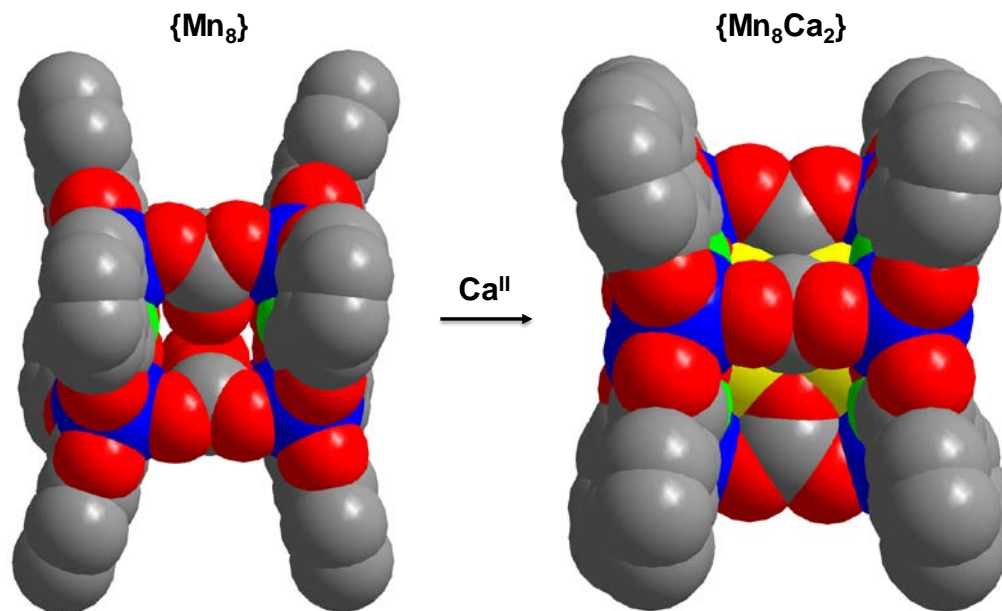


**Figure 5.** Space-filling representations of the ‘vacant’  $\{\text{Mn}_8\}$  molecular ‘capsule’ of **4** (left) and its complete  $\{\text{Mn}_8\text{Ca}_2\}$  structure (right), as resulted from the filling of the cavity by two  $\text{Ca}^{\text{II}}$  atoms. Color scheme as in Figure 4.

Considering the fast-developing field of heterometallic Mn-Ca chemistry, we felt timely to report in Table 3 all the structurally characterized Mn-Ca cluster compounds reported to date, together with some of the most significant features from a bioinorganic perspective (i.e., metal stoichiometry, Mn oxidation states and overall magnetic response). It becomes apparent that complexes **1-4** are quite unique in their metal ions stoichiometries, topological arrangements, oxidation state descriptions and the nature of the ligands bound to the metal ions.

**Table 3. Chemical Formulae, Structural Details and Ground State *S* Values for the Mn-Ca Cluster Compounds Reported to Date**

Formula <sup>a,b</sup>	Metal Stoichiometry	Mn Oxidation States	<i>S</i> <sup>c</sup>	Ref.
[Mn <sub>3</sub> CaO <sub>3</sub> (OH)(L1)(ON <sub>4</sub> O)(O <sub>2</sub> CMe)] <sup>+</sup>	3Mn:1Ca	3 Mn <sup>IV</sup>	n.r.	55
[Mn <sub>3</sub> CaO <sub>4</sub> (L1)(ON <sub>4</sub> O)(O <sub>2</sub> CMe)]	3Mn:1Ca	3 Mn <sup>IV</sup>	n.r.	55
[Mn <sub>3</sub> CaAgO <sub>4</sub> (L1)(ON <sub>4</sub> O)(O <sub>2</sub> CMe)(OTf)]	3Mn:1Ca	3 Mn <sup>IV</sup>	n.r.	55
[Mn <sub>3</sub> CaO <sub>4</sub> (L1)(O <sub>2</sub> CMe) <sub>3</sub> (THF)]	3Mn:1Ca	3 Mn <sup>IV</sup>	n.r.	22
[Mn <sub>6</sub> CaO <sub>2</sub> (L1) <sub>2</sub> (O <sub>2</sub> CMe) <sub>6</sub> ] <sup>2+</sup>	6Mn:1Ca	2 Mn <sup>II</sup> , 4 Mn <sup>III</sup>	n.r.	22
[Mn <sub>3</sub> CaO <sub>2</sub> (L1)(O <sub>2</sub> CMe) <sub>2</sub> (DME)(OTf)] <sup>2+</sup>	3Mn:1Ca	2 Mn <sup>III</sup> , 1 Mn <sup>IV</sup>	11/2	56
[Mn <sub>3</sub> CaO <sub>2</sub> (L1)(O <sub>2</sub> CMe) <sub>2</sub> (DME)(OTf)] <sup>+</sup>	3Mn:1Ca	3 Mn <sup>III</sup>	n.r.	56
[Mn <sub>3</sub> CaO <sub>2</sub> (L1)(O <sub>2</sub> CMe) <sub>2</sub> (H <sub>2</sub> O) <sub>3</sub> ] <sup>3+</sup>	3Mn:1Ca	2 Mn <sup>III</sup> , 1 Mn <sup>IV</sup>	n.r.	56
[Mn <sub>3</sub> CaNaO(L2) <sub>3</sub> (N <sub>3</sub> ) <sub>3</sub> (MeOH)] <sup>+</sup>	3Mn:1Ca	3 Mn <sup>III</sup>	n.r.	57
[Mn <sub>13</sub> Ca <sub>2</sub> O <sub>10</sub> (OH) <sub>2</sub> (OMe) <sub>2</sub> (O <sub>2</sub> CPh) <sub>18</sub> (H <sub>2</sub> O) <sub>4</sub> ]	13Mn:2Ca	2 Mn <sup>II</sup> , 10 Mn <sup>III</sup> , 1 Mn <sup>IV</sup>	5/2	58
[Mn <sub>4</sub> CaO <sub>4</sub> (O <sub>2</sub> CBu <sup>t</sup> ) <sub>8</sub> (Bu <sup>t</sup> CO <sub>2</sub> H) <sub>2</sub> (py)]	4Mn:1Ca	2 Mn <sup>III</sup> , 2 Mn <sup>IV</sup>	n.r.	23
[Mn <sub>4</sub> CaO <sub>4</sub> (O <sub>2</sub> CBu <sup>t</sup> ) <sub>8</sub> (Bu <sup>t</sup> CO <sub>2</sub> H)(py) <sub>2</sub> ]	4Mn:1Ca	2 Mn <sup>III</sup> , 2 Mn <sup>IV</sup>	n.r.	23
[Mn <sub>4</sub> CaO <sub>4</sub> (O <sub>2</sub> CBu <sup>t</sup> ) <sub>8</sub> (Bu <sup>t</sup> CO <sub>2</sub> H) <sub>2</sub> (qn)]	4Mn:1Ca	2 Mn <sup>III</sup> , 2 Mn <sup>IV</sup>	n.r.	23
[Mn <sub>6</sub> Ca <sub>2</sub> O <sub>2</sub> (Me-sao) <sub>6</sub> (O <sub>2</sub> CEt) <sub>6</sub> (H <sub>2</sub> O) <sub>2</sub> ] <sub>n</sub>	6Mn:2Ca	6 Mn <sup>III</sup>	4	59
[Mn <sub>4</sub> CaOCl <sub>3</sub> (L3) <sub>3</sub> (O <sub>2</sub> CMe)(H <sub>2</sub> O) <sub>1.5</sub> (MeOH) <sub>0.3</sub> ] <sup>+</sup>	4Mn:1Ca	1 Mn <sup>II</sup> , 3 Mn <sup>III</sup>	1/2	60
[Mn <sub>2</sub> Ca <sub>2</sub> (L4) <sub>2</sub> (DMF) <sub>4</sub> ]	2Mn:2Ca	2 Mn <sup>II</sup>	n.r.	61
[MnCa <sub>2</sub> (L4H) <sub>2</sub> (DMF) <sub>4</sub> ]	1Mn:2Ca	1 Mn <sup>II</sup>	n.r.	61
[Mn <sub>3</sub> CaNa(sal) <sub>6</sub> (H <sub>2</sub> O) <sub>6</sub> ] <sub>n</sub>	3Mn:1Ca	3 Mn <sup>III</sup>	n.r.	62
[Mn <sub>2</sub> Ca <sub>2</sub> (tpaa) <sub>2</sub> (H <sub>2</sub> O) <sub>12</sub> ][Mn(tpaa)] <sub>2</sub>	2Mn:2Ca	2 Mn <sup>II</sup>	n.r.	63
[MnCa <sub>2</sub> (Hcit) <sub>2</sub> (H <sub>2</sub> O) <sub>4</sub> ] <sub>n</sub>	1Mn:2Ca	1 Mn <sup>II</sup>	n.r.	64

$[\text{Mn}_6\text{Ca}_2\text{O}_9(\text{O}_2\text{CBu}^t)_{10}(\text{H}_2\text{O})_4]$	6Mn:2Ca	6 Mn <sup>IV</sup>	n.r.	65
$[\text{Mn}_6\text{Ca}_2\text{O}_9(\text{O}_2\text{CBu}^t)_{10}(\text{H}_2\text{O})_3(\text{CH}_3\text{CO}_2\text{C}_2\text{H}_5)]$	6Mn:2Ca	6 Mn <sup>IV</sup>	n.r.	65
$[\text{Mn}_6\text{Ca}_2\text{O}_9(\text{O}_2\text{CBu}^t)_{11}][\text{Mn}_3\text{O}(\text{O}_2\text{CBu}^t)_6(\text{py})_3]$	6Mn:2Ca	6 Mn <sup>IV</sup>	n.r.	65
$[\text{Mn}_4\text{Ca}_2\text{Cl}_4(\text{OEtOMe})_8]$	4Mn:2Ca	4 Mn <sup>II</sup>	n.r.	66
$[\text{MnCa}_2(\text{O}_2\text{CCCl}_2)_6(\text{bipy})_2(\text{H}_2\text{O})(\text{MeOH})]$	1Mn:2Ca	1 Mn <sup>II</sup>	5/2	67
$[\text{Mn}_3\text{Ca}_2\text{O}_4(\text{O}_2\text{CBu}^t)_8(\text{Bu}^t\text{CO}_2\text{H})_4]$	3Mn:2Ca	3 Mn <sup>IV</sup>	9/2	24
$[\text{Mn}_6\text{Ca}_2\text{O}_9(\text{O}_2\text{CPhBu}^t)_{10}(\text{Bu}^t\text{PhCO}_2\text{H})_5]$	6Mn:2Ca	6 Mn <sup>IV</sup>	0	68
$[\text{Mn}_4\text{Ca}(\text{O}_2\text{CPh})_4(\text{shi})_4]^{2-}$	4Mn:1Ca	4 Mn <sup>III</sup>	0	26
$[\text{Mn}_4\text{Ca}(\text{L5})_4(\text{shi})_4]^{2-}$	4Mn:1Ca	4 Mn <sup>III</sup>	0	26
$[\text{Mn}_4\text{Ca}(\text{L6})_4(\text{shi})_4]^{2-}$	4Mn:1Ca	4 Mn <sup>III</sup>	0	26
$[\text{Mn}_4\text{Ca}(\text{L6})_4(\text{shi})_4(\text{shiH}_2)_2]^{4-}$	4Mn:1Ca	4 Mn <sup>III</sup>	0	26
$[\text{Mn}_4\text{Ca}(\text{L7})_4(\text{shi})_4]^{2-}$	4Mn:1Ca	4 Mn <sup>III</sup>	0	26
$[\text{Mn}_4\text{Ca}_2(\text{O}_2\text{CPh})_4(\text{shi})_4(\text{H}_2\text{O})_2(\text{Me}_2\text{CO})_2]$ ( <b>1</b> )	4Mn:2Ca	4 Mn <sup>III</sup>	0	t.w.
$[\text{Mn}_6\text{Ca}_2\text{Cl}_2(\text{O}_2\text{CPh})_7(\text{shi})_4(\text{py})_4]^-$ ( <b>2</b> )	6Mn:2Ca	2 Mn <sup>II</sup> , 4 Mn <sup>III</sup>	0	t.w.
$[\text{Mn}_8\text{Ca}(\text{OEt})_2(\text{shi})_{10}(\text{EtOH})_2]^{2-}$ ( <b>3</b> )	8Mn:1Ca	4 Mn <sup>III</sup> , 4 Mn <sup>IV</sup>	0	t.w.
$[\text{Mn}_8\text{Ca}_2(\text{CO}_3)(\text{shi})_8]^{4-}$ ( <b>4</b> )	8Mn:2Ca	8 Mn <sup>III</sup>	0	t.w.

<sup>a</sup> Excluding all lattice solvate molecules and counterions.

<sup>b</sup> Abbreviations: n.r. = not reported; t.w. = this work; L1H<sub>3</sub> = 1,3,5-tris(2-di(2'-pyridyl)hydroxymethylphenyl)benzene; THF = tetrahydrofuran; HON<sub>4</sub>OH = N,N'-dimethyl-N,N'-diacetylenediamine dioxime; OTf<sup>-</sup> = trifluoromethanesulfonate; L2H<sub>3</sub> = 2-(2,3-dihydroxypropyliminomethyl)-6-methoxyphenol; L3H<sub>2</sub> = 2-[(2-hydroxypropyl)imino]methyl]-6-methoxyphenol; L4H<sub>4</sub> = *p-t*-butylthiacalix[4]arene; DME = 1,2-dimethoxyethane; qn = isoquinoline; Me-saoH<sub>2</sub> = 2-hydroxyphenylethanone oxime; L5H = 2-naphthoic acid; L6H = 9-anthracenecarboxylic acid; L7H = 1-pyrenecarboxylic acid; DMF = dimethylformamide; H<sub>2</sub>sal = salicylic acid; H<sub>3</sub>tpaa = 6,6',6''-nitrilotris(methylene)tripicolinic acid; H<sub>4</sub>cit = citric acid; MeOEtOH = 2-methoxyethanol; bipy = 2,2'-bipyridine; Bu<sup>t</sup>PhCO<sub>2</sub>H = *p*-tert-butylbenzoic acid.

<sup>c</sup> From magnetic susceptibility data.

**Solid-State Magnetic Susceptibility Studies.** Variable-temperature direct current (dc) magnetic susceptibility measurements were performed on powdered polycrystalline samples of analytically pure complexes **1**·2H<sub>2</sub>O, **2**, **3**·2H<sub>2</sub>O, and **4**·2CHCl<sub>3</sub>, restrained in eicosane to prevent torquing, in a 1 kG (0.1 T) field and in the 5.0-300 K range. The data are shown as  $\chi_{\text{M}}T$  versus  $T$  plots in Figure 6. All complexes show very similar magnetic responses in terms of exhibiting a continuous decrease of their  $\chi_{\text{M}}T$  products from 300 to 5 K. This is clearly due to the antiferromagnetic exchange interactions between the paramagnetic metal centers, undoubtedly propagated by the oximate bridges with very large (close to linearity) Mn-O-N-Mn torsion angles. This behavior is consistent with all previously characterized Mn-oximate complexes with large torsion angles.<sup>26,69</sup> More specifically, the  $\chi_{\text{M}}T$  product for all four complexes steadily decreases from 9.28 (**1**), 17.53 (**2**), 15.03 (**3**), and 20.16 (**4**) cm<sup>3</sup>Kmol<sup>-1</sup> at 300 K to 0.74 (**1**), 0.87 (**2**), 0.88 (**3**), and 0.91 (**4**) cm<sup>3</sup>Kmol<sup>-1</sup> at 5.0 K. The 300 K values are less than the spin-only ( $g = 2$ ) values of 12.00 (**1**), 20.75 (**2**), 19.50 (**3**), and 24.00 (**4**) cm<sup>3</sup>Kmol<sup>-1</sup> for the corresponding number of non-interacting Mn<sup>III</sup> (**1** and **4**), Mn<sup>II/III</sup> (**2**), and Mn<sup>III/IV</sup> (**3**) ions. Given the very small  $\chi_{\text{M}}T$  values for all complexes at low temperatures and the topological arrangement of the Mn atoms, it is very likely that compounds **1-4** all possess  $S = 0$  spin ground state values. This was confirmed quantitatively by determining the individual pairwise exchange parameters  $J_{ij}$  between Mn<sub>*i*</sub>Mn<sub>*j*</sub> pairs within the magnetic cores, when the overall topology and symmetry of the compound allowed us to do so.

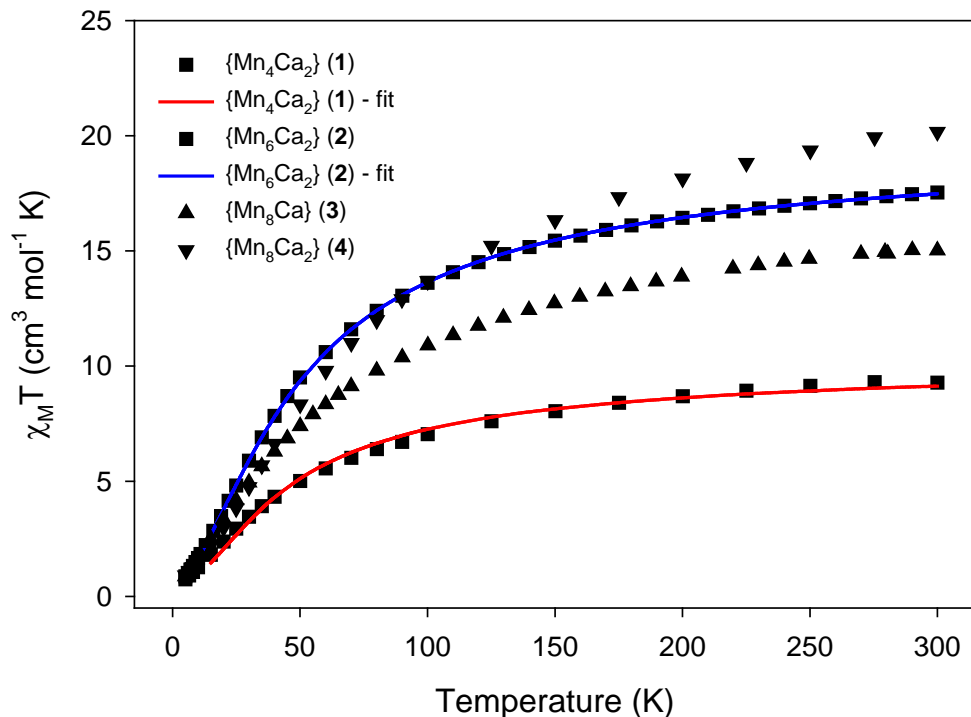


**Figure 6.**  $\chi_M T$  vs  $T$  plots for complex **1-4** at 0.1 T direct current (dc) field. The red and blue solid lines are the fit of the corresponding data; see the text for the fit parameters.

To this end, the  $\chi_M T$  versus  $T$  data for complex **1** were fit to the theoretical expression for a  $\{\text{Mn}^{\text{III}}_4\}$  square using the isotropic Heisenberg spin Hamiltonian given by eq 5.

$$\mathcal{H} = -2J(\hat{S}_1 \cdot \hat{S}_2 + \hat{S}_2 \cdot \hat{S}_3 + \hat{S}_3 \cdot \hat{S}_4 + \hat{S}_1 \cdot \hat{S}_4) \quad (5)$$

Considering the very similar Mn-O-N-Mn torsion angles and Mn $\cdots$ Mn separations within the  $\text{Mn}_4$  square, all interactions between neighboring  $\text{Mn}^{\text{III}}$  atoms were considered as equivalent (1- $J$  model). The fit parameters were thus  $J$  and  $g$ . A good fit of the experimental data (red solid line in Figure 6) in the temperature range 300-15 K was obtained using the program PHI ( $\mathcal{H} = -2J_{ij}\hat{S}_i \cdot \hat{S}_j$  convention).<sup>70</sup> The best-fit parameters were:  $J = -2.94(1) \text{ cm}^{-1}$  and  $g = 1.96(1)$ , in very good agreement with the previously reported  $\{\text{Mn}^{\text{III}}_4\text{Ca}\}$  complexes possessing square pyramidal

topologies. Data below 15 K were omitted to avoid effects from Zeeman interactions, magnetic anisotropy and crystal structure disorders; these are all factors that are not included in the above model.<sup>26</sup>**Error! Bookmark not defined.** The fit of the data indicates an  $S = 0$  ground state with an  $S = 1$  first excited state lying  $5.88 \text{ cm}^{-1}$  higher in energy. Attempts to include a  $D$  term in the fitting process and/or a second  $J$ -coupling constant, to account for any non-zero next-nearest neighbor interactions across the diagonal Mn sites, failed to give us any better low-temperature fits.

For the  $\{\text{Mn}^{\text{II}}_2\text{Mn}^{\text{III}}_4\text{Ca}_2\}$  complex **2**, we employed a similar Heisenberg spin Hamiltonian (eq 6), but this time two coupling constants were included to account for the interactions between the  $\text{Mn}^{\text{III}}$  atoms within the  $\{\text{Mn}_4\}$  square ( $J_1$ ), as promoted by the oximate bridges, and the interaction between the two carboxylate-bridged  $\text{Mn}^{\text{II}}$  atoms ( $J_2$ ). The best-fit parameters were:  $J_1 = -2.88(1) \text{ cm}^{-1}$ ,  $J_2 = -4.13(1) \text{ cm}^{-1}$ , and  $g = 1.95(1)$ , and these were derived from the program PHI for the entire temperature range (blue solid line in Figure 6), thus confirming the overall antiferromagnetic response of the compound and the stabilization of an  $S = 0$  spin ground state.

$$\mathcal{H} = -2J_1(\hat{S}_2 \cdot \hat{S}_3 + \hat{S}_3 \cdot \hat{S}_{2'} + \hat{S}_{2'} \cdot \hat{S}_{3'} + \hat{S}_{3'} \cdot \hat{S}_2) - 2J_2(\hat{S}_1 \cdot \hat{S}_{1'}) \quad (6)$$

The employment of a third  $J$ -coupling constant to consider any possible interaction between the  $\text{Mn}^{\text{II}}$  and  $\text{Mn}^{\text{III}}$  atoms gave us a negligible value ( $\sim 0 \text{ cm}^{-1}$ ). This is reasonable since the  $\text{Mn}^{\text{II}}$  and  $\text{Mn}^{\text{III}}$  atoms in **2** are solely bridged by the  $\text{Cl}^-$  groups, which are expected to provide a very weak to negligible superexchange magnetic pathway when forming an almost linear angle between the metal centers [ $\text{Mn}(1)\text{-Cl}(1)\text{-Mn}(3') = 169.8(1)^\circ$ ], and the bonding is weak as well [ $\text{Mn}(1)\text{-Cl}(1) = 2.486(1) \text{ \AA}$  and  $\text{Mn}(3)\text{-Cl}(1) = 2.870(3) \text{ \AA}$ ].

The larger nuclearities and low symmetries of complexes **3** and **4** rendered the fitting of the magnetic data impossible. A powerful complement to dc studies for determining the ground state of a system is alternating current (ac) magnetic susceptibility measurements, which preclude any complications arising from the presence of a dc field. These were performed for both **3** and **4** in a 3.5 G ac field oscillating at different frequencies. The in-phase susceptibility ( $\chi_M'$ ) is shown as  $\chi_M'T$  versus  $T$  plots in Figure S5, and reveals some pertinent and common features for both complexes **3** and **4**: (i)  $\chi_M'T$  decreases linearly with decreasing temperature in the 1.8-14 K range, indicating the depopulation of a high density of excited states with spin  $S$  greater than that of the ground state; (ii) linear extrapolation of the  $\chi_M'T$  data down to 0 K gives a value of  $\sim 0 \text{ cm}^3\text{Kmol}^{-1}$  for both **3** and **4**, indicative of  $S = 0$  ground states.

**Relevance of Complexes 1-4 to Different Oxidation States of OEC: A Qualitative Approach.** A qualitative and brief discussion of the relevance of complexes **1-4** to some species of the native OEC is herein attempted. In addition to the bridging/chelating  $\text{shi}^{3-}$  ligand, most of the reported compounds contain carboxylate, chloride, water, and/or carbonate groups akin to the coordination environment of the metal ions in the native enzyme. We recognize that within the structures of **1-4**, the Mn $\cdots$ Mn (between closest neighbors) and Mn $\cdots$ Ca separations span the range 4.623-4.652 and 3.680-3.773 (**1**), 4.624-6.283 and 3.620-3.856 Å (**2**), 3.180-6.639 and 3.545-4.048 Å (**3**), and 4.612-6.122 and 3.601-3.635 Å (**4**), respectively; these values are significantly larger than the corresponding values of 2.7-3.3 and  $\sim 3.4$  Å for the OEC in PSII. This is clearly due to the absence of bridging oxido groups and the presence of Mn<sup>II</sup>/Mn<sup>III</sup> atoms within **1-4**. However, the structures of the reported compounds may be of some relevance to the OEC in other ways. Since the  $S_1$  Kok state of the OEC occurs at the 2Mn<sup>III</sup>,2Mn<sup>IV</sup> oxidation level

with a ground state spin of  $S = 0$ , then the  $\text{Mn}^{\text{III}}_4\text{Mn}^{\text{IV}}_4$  level of **3** could be related to this  $S_1$  state. In contrast, the lower  $\text{Mn}^{\text{III}}_4$ ,  $\text{Mn}^{\text{II}}_2\text{Mn}^{\text{III}}_4$  and  $\text{Mn}^{\text{III}}_8$  levels of **1**, **2** and **4**, respectively, would place them at the  $S_{-1}$  or other reduced states of the catalytic cycle. Hydrazine ( $\text{N}_2\text{H}_4$ ), hydroxylamine ( $\text{NH}_2\text{OH}$ ) and nitric oxide can reduce the OEC to  $S_{-1}$ ,  $S_{-2}$  and even  $S_{-3}$  states.<sup>71</sup> These are not involved in the water oxidation catalytic cycle, but may be related to intermediates during the *in vivo* assembly of the OEC. Assuming these involve Mn-based reductions, then they would be at the  $4\text{Mn}^{\text{III}}$ ,  $\text{Mn}^{\text{II}}, 3\text{Mn}^{\text{III}}$  and  $2\text{Mn}^{\text{II}}, 2\text{Mn}^{\text{III}}$  levels, respectively; an EPR signal assignable to a  $\text{Mn}^{\text{II}}\text{Mn}^{\text{III}}$  subunit has been detected for  $S_{-2}$ .<sup>72</sup> Furthermore, the similarity between the oximate N-O bridging unit of  $\text{shi}^{3-}$  within **1-4** and the M-N-O-M unit found in hydroxylamine-bridged metal complexes<sup>73</sup> is interesting and suggests that **1-4** may be providing insights into the type of subunits that might be generated upon reduction of the OEC with  $\text{NH}_2\text{OH}$ .

## CONCLUSIONS

In conclusion, we have shown that salicylhydroxime is a versatile chelating/bridging ligand that can support the formation of heterometallic Mn-Ca clusters with unprecedented topologies, metal stoichiometries and oxidation state descriptions. The reaction schemes employed in this work were quite diverse, ranging from the use of  $\{\text{Mn}^{\text{III}}_3\}$  and  $\{\text{Mn}^{\text{II/III}}_3\}$  oxido/carboxylate-based triangles to simple  $\text{Mn}^{\text{II}}$  and  $\text{Ca}^{\text{II}}$  starting materials, and the resulting crystalline products were proved to exhibit different structural motifs and ancillary bridging ligands, such as  $\text{PhCO}_2^-$ ,  $\text{EtO}^-$ ,  $\text{Cl}^-$  and  $\text{CO}_3^{2-}$ . The combined results also demonstrate the ability of  $\text{shi}^{3-}$  to stabilize Mn ions in high oxidation states (i.e.,  $\text{Mn}^{\text{IV}}$ ) without requiring the support of oxido groups. It must be admitted that the cores and metal stoichiometries of **1-4** are different from the extended



{Mn<sub>4</sub>Ca} cubane core of the native OEC. This, however, does not preclude some relevance of the reported compounds to both the high-valent scheme (Mn<sup>III</sup><sub>4</sub>Mn<sup>IV</sup><sub>4</sub>; **3**) and lower oxidation level species (**1**, **2**, and **4**) that are intermediates during assembly of the OEC *in vivo*, or those generated by treatment of the OEC with strong reducing agents.

We are still seeking ways and new synthetic conditions to stabilize Mn-Ca/shi<sup>3-</sup> complexes with coordinated and bridging O<sup>2-</sup> groups, as a means of obtaining heterometallic cluster compounds with more relevance to the S<sub>0</sub>-S<sub>3</sub> states within the high-valent scheme of the catalytic Kok cycle. In addition, work in progress includes the synthesis and systematic investigation of various new hydroxamic acids and oxime-based ligands in Mn-Ca coordination chemistry. Finally, the {Mn<sub>4</sub>Ca<sub>2</sub>} octahedral arrangement of **1** is very similar to the one seen before in Mn-Ce chemistry albeit with different bridging and ancillary ligands.<sup>74</sup> This is important when targeting for the deliberate replacement of Ca<sup>II</sup> atoms by paramagnetic and anisotropic 4*f*-metal ions in an attempt to synthesize molecule-based magnets.

## ASSOCIATED CONTENT

**Supporting Information.** Crystallographic data for all reported compounds in CIF formats, selected interatomic distances and angles, coordination polyhedra for all Ca atoms, and  $\chi_M T$  versus *T*. This material is available free of charge via the Internet at <http://pubs.acs.org>. Crystallographic data (excluding structure factors) for the structures reported in this work have been deposited to the Cambridge Crystallographic Data Centre (CCDC) as supplementary publication numbers: CCDC-1559579 (**1**·3Me<sub>2</sub>CO·2.8H<sub>2</sub>O), 1559399 (**2**·2Et<sub>2</sub>O·CH<sub>2</sub>Cl<sub>2</sub>), 1559398 (**3**·3EtOH·H<sub>2</sub>O) and 1559957 (**4**·9CHCl<sub>3</sub>). Copies of these data can be obtained free of

charge on application to CCDC, 12 Union Road, Cambridge CB2 2EZ, U.K.; FAX: (+44) 1223 336033, or online via [www.ccdc.cam.ac.uk/data\\_request/cif](http://www.ccdc.cam.ac.uk/data_request/cif) or by emailing [data\\_request@ccdc.cam.ac.uk](mailto:data_request@ccdc.cam.ac.uk).

## **AUTHOR INFORMATION**

### **Corresponding Author**

\*E-mail: [tstamatatos@brocku.ca](mailto:tstamatatos@brocku.ca)

### **Notes**

The authors declare no competing financial interest.

## **ACKNOWLEDGMENTS**

This work was supported by NSERC-DG (Th. C. S), ERA (Th. C. S), Brock University (Chancellor's Chair for Research Excellence; Th. C. S), and NSF grant CHE-1410394 (to G. C). A. A. would like to thank the Queen Elizabeth II Graduate Scholarships in Science and Technology for supporting this work. L. C.-S. acknowledges financial support from FCT/MCTES (Fundação para a Ciência e a Tecnologia / Ministério da Ciência, Tecnologia e Ensino Superior, Portugal) with national funds and was also co-financed by FEDER (Fundo Europeu de Desenvolvimento Regional, European Union) under the partnership agreement PT2020, through the research centre REQUIMTE-LAQV (UID/QUI/50006/2013 - POCI/01/0145/FEDER/007265). A. E. acknowledges financial support from Ministerio de Economía y Competitividad, Project CTQ2015-63614-P. The Advanced Light Source is

supported by the Director, Office of Science, Office of Basic Energy Sciences, of the U.S. Department of Energy under Contract No. DE-AC02-05CH11231.

## REFERENCES

---

<sup>1</sup> (a) Wydrzynski, T.; Satoh, K. *The Light-Driven Water: Plastoquinone Oxidoreductase*; Springer: Dordrecht, **2005**; Vol. 22. (b) McEvoy, J. P.; Brudvig, G. W. Water-Splitting Chemistry of Photosystem II. *Chem. Rev.* **2006**, *106*, 4455-4483. (c) Yano, J.; Yachandra, V. Mn<sub>4</sub>Ca Cluster in Photosynthesis: Where and How Water is Oxidized to Dioxygen. *Chem. Rev.* **2014**, *114*, 4175-4205.

<sup>2</sup> For representative references, see: (a) Mukhopadhyay, S.; Mandal, S. K.; Bhaduri, S.; Armstrong, W. H. Manganese Clusters with Relevance to Photosystem II. *Chem. Rev.* **2004**, *104*, 3981–4026. (b) Pecoraro, V. L.; Hsieh, W.-Y. In Search of Elusive High-Valent Manganese Species That Evaluate Mechanisms of Photosynthetic Water Oxidation. *Inorg. Chem.* **2008**, *47*, 1765–1778. (c) Meelich, K.; Zaleski, C. M.; Pecoraro, V. L. Using small molecule complexes to elucidate features of photosynthetic water oxidation. *Philos. Trans. R. Soc. B* **2008**, *363*, 1271–1281.

<sup>3</sup> (a) Barber, J. Photosynthetic energy conversion: natural and artificial. *Chem. Soc. Rev.* **2009**, *38*, 185–196. (b) Nocera, D. G. The Artificial Leaf. *Acc. Chem. Res.* **2012**, *45*, 767–776. (c) Cox, N.; Pantazis, D. A.; Neese, F.; Lubitz, W. Artificial photosynthesis: understanding water splitting in nature. *Interface Focus* **2015**, *5*, 20150009.

---

<sup>4</sup> Yano, J.; Kern, J.; Sauer, K.; Latimer, M. J.; Pushkar, Y.; Biesiadka, J.; Loll, B.; Saenger, W.; Messinger, J.; Zouni, A.; Yachandra, V. K. Where Water Is Oxidized to Dioxygen: Structure of the Photosynthetic Mn<sub>4</sub>Ca Cluster. *Science* **2006**, *314*, 821-825.

<sup>5</sup> (a) Barber, J. Mn<sub>4</sub>Ca Cluster of Photosynthetic Oxygen-Evolving Center: Structure, Function and Evolution. *Biochemistry* **2016**, *55*, 5901–5906. (b) Shen, J.- R. The Structure of Photosystem II and the Mechanism of Water Oxidation in Photosynthesis. *Annu. Rev. Plant Biol.* **2015**, *66*, 23–48.

<sup>6</sup> (a) Zouni, A.; Witt, H.- T.; Kern, J.; Fromme, P.; Krauß, N.; Saenger, W.; Orth, P. Crystal Structure of Photosystem II from *Synechococcus Elongatus* at 3.8 Å Resolution. *Nature* **2001**, *409*, 739–743. (b) Peloquin, J. M.; Campbell, K. A.; Randall, D. W.; Evanchik, M. A.; Pecoraro, V. L.; Armstrong, W. H.; Britt, R. D. <sup>55</sup>Mn ENDOR of the S<sub>2</sub>-State Multiline EPR Signal of Photosystem II: Implications on the Structure of the Tetranuclear Mn Cluster. *J. Am. Chem. Soc.* **2000**, *122*, 10926-10942. (c) Pantazis, D. A.; Ames, W.; Cox, N.; Lubitz, W.; Neese, F. Two Interconvertible Structures that Explain the Spectroscopic Properties of the Oxygen-Evolving Complex of Photosystem II in the S<sub>2</sub> State. *Angew. Chem. Int. Ed.* **2012**, *51*, 9935-9940.

<sup>7</sup> Brynda, M.; Britt, R. D. The Manganese-Calcium Cluster of the Oxygen-Evolving System: Synthetic Models, EPR Studies, and Electronic Structure Calculations. In *Metals in Biology: Applications of High-Resolution EPR to Metalloenzymes*; Hanson, G.; Berliner, L., Eds.; Springer: New York, NY, **2010**, pp. 203–271.

<sup>8</sup> (a) Kok, B.; Forbush, B.; McGloin, M. Cooperation of Charges in Photosynthetic O<sub>2</sub> Evolution-I. A Linear Four Step Mechanism. *Photochem. Photobiol.* **1970**, *11*, 457-475. (b) Joliot, P.; Barbieri G.; Chabaud, R. Un Nouveau Modele Des Centees Photochimiques Du System II. *Photochem. Photobiol.* **1969**, *10*, 309–329.

- 
- <sup>9</sup> (a) Visser, H.; Anxolabéhère-Mallart, E.; Bergmann, U.; Glatzel, P.; Robblee, J. H.; Cramer, S. P.; Girerd, J.- J.; Sauer, K.; Klein, M. P.; Yachandra, V. K. Mn K-Edge XANES and K $\beta$  XES Studies of Two Mn-Oxo Binuclear Complexes: Investigation of Three Different Oxidation States Relevant to the Oxygen-Evolving Complex of Photosystem II. *J. Am. Chem. Soc.* **2001**, *123*, 7031-7039. (b) Pecoraro, V. L.; Baldwin, M. J.; Caudle, M. T.; Hsieh, W.- Y.; Law, N. A. A proposal for water oxidation in photosystem II. *Pure & Appl. Chem.* **1998**, *70*, 925-929.
- <sup>10</sup> (a) Haumann, M.; Liebisch, P.; Müller, C.; Barra, M.; Grabolle, M.; Dau, H. Photosynthetic O<sub>2</sub> Formation Tracked by Time-Resolved X-ray Experiments. *Science* **2005**, *310*, 1019-1021. (b) Kolling, D. R. J.; Cox, N.; Ananyev, G. M.; Pace, R. J.; Dismukes, G. C. What Are the Oxidation States of Manganese Required to Catalyze Photosynthetic Water Oxidation? *Biophys. J.* **2012**, *103*, 313-322.
- <sup>11</sup> Loll, B.; Kern, J.; Saenger, W.; Zouni, A.; Biesiadka, J. Towards complete cofactor arrangement in the 3.0 Å resolution structure of photosystem II. *Nature* **2005**, *438*, 1040-1044.
- <sup>12</sup> Tsui, E. Y.; Kanady, J. S.; Agapie, T. Synthetic Cluster Models of Biological and Heterogeneous Manganese Catalysts for O<sub>2</sub> Evolution. *Inorg. Chem.* **2013**, *52*, 13833-13848.
- <sup>13</sup> Umena, Y.; Kawakami, K.; Shen, J.- R.; Kamiya, N. Crystal structure of oxygen-evolving photosystem II at a resolution of 1.9 Å. *Nature* **2011**, *473*, 55-60.
- <sup>14</sup> Krewald, V.; Retegan, M.; Cox, N.; Messinger, J.; Lubitz, W.; DeBeer, S.; Neese, F.; Pantazis, D. A. Metal oxidation states in biological water splitting. *Chem. Sci.* **2015**, *6*, 1676–1695.
- <sup>15</sup> (a) Miller, A.- F.; Brudvig, G. W. Electron-Transfer Events Leading to Reconstitution of Oxygen-Evolution Activity in Manganese-Depleted Photosystem II Membranes. *Biochemistry* **1990**, *29*, 1385-1392. (b) Burnap, R. L. D1 protein processing and Mn cluster assembly in light of the emerging Photosystem II structure. *Phys. Chem. Chem. Phys.* **2004**, *6*, 4803-4809.

- 
- <sup>16</sup> (a) Campbell, K. A.; Force, D. A.; Nixon, P. J.; Dole, F.; Diner, B. A.; Britt, R. D. Dual-Mode EPR Detects the Initial Intermediate in Photoassembly of the Photosystem II Mn Cluster: The Influence of Amino Acid Residue 170 of the D1 Polypeptide on Mn Coordination. *J. Am. Chem. Soc.* **2000**, *122*, 3754-3761. (b) Dasgupta, J.; Ananyev, G. M.; Dismukes, G. C. Photoassembly of the water-oxidizing complex in photosystem II. *Coord. Chem. Rev.* **2008**, *252*, 347-360.
- <sup>17</sup> Brudvig, G. W.; Beck, W. F. Biomimetic Oxidations Catalyzed by Transition Metal Complexes. In *Manganese Redox Enzymes*; Pecoraro, V. L., Ed.; VCH Publishers, Inc., New York, **1992**, pp. 119-140.
- <sup>18</sup> Schansker, G.; Goussias, C.; Petrouleas V.; Rutherford, A. W. Reduction of the Mn Cluster of the Water-Oxidizing Enzyme by Nitric Oxide: Formation of an S<sub>2</sub> State. *Biochemistry* **2002**, *41*, 3057–3064.
- <sup>19</sup> Kanady, J. S.; Tran, R.; Stull, J. A.; Lu, L.; Stich, T. A.; Day, M. W.; Yano, J.; Britt, R. D.; Agapie, T. Role of oxido incorporation and ligand lability in expanding redox accessibility of structurally related Mn<sub>4</sub> cluster. *Chem. Sci.* **2013**, *4*, 3986-3996.
- <sup>20</sup> For recent reviews in polynuclear Mn clusters, see: (a) Kostakis, G. E.; Blatov, V. A.; Proserpio, D. M. A method for topological analysis of high nuclearity coordination clusters and its application to Mn coordination compounds. *Dalton Trans.* **2012**, *41*, 4634-4640. (b) Aromí, G.; Brechin, E. K. Synthesis of 3d Metallic Single-Molecule Magnets. *Struct. Bond.* **2006**, *122*, 1-67. (c) Papatriantafyllopoulou, C.; Moushi, E. E.; Christou, G.; Tasiopoulos, A. J. Filling the gap between the quantum and classical worlds of nanoscale magnetism: giant molecular aggregates based on paramagnetic 3d metal ions. *Chem. Soc. Rev.* **2016**, *45*, 1597-1628.

- 
- <sup>21</sup> Gerey, B.; Gouré, E.; Fortage, J.; Pécaut, J.; Collomb, M.- N. Manganese-calcium/strontium heterometallic compounds and their relevance for the oxygen-evolving center of photosystem II. *Coord. Chem. Rev.* **2016**, *319*, 1-24.
- <sup>22</sup> Kanady, J. S.; Tsui, E. Y.; Day, M. W.; Agapie, T. A Synthetic Model of the Mn<sub>3</sub>Ca Subsite of the Oxygen-Evolving Complex in Photosystem II. *Science* **2011**, *333*, 733-736.
- <sup>23</sup> Zhang, C.; Chen, C.; Dong, H.; Shen, J.- R.; Dau, H.; Zhao, J. A synthetic Mn<sub>4</sub>Ca-cluster mimicking the oxygen-evolving center of photosynthesis. *Science* **2015**, *348*, 690-693.
- <sup>24</sup> Mukherjee, S.; Stull, J. A.; Yano, J.; Stamatatos, T. C.; Pringouri, K.; Stich, T. A.; Abboud, K. A.; Britt, R. D.; Yachandra, V. K.; Christou, G. Synthetic model of the asymmetric [Mn<sub>3</sub>CaO<sub>4</sub>] cubane core of the oxygen-evolving complex of photosystem II. *Proc. Natl. Acad. Sci. U. S. A.* **2012**, *109*, 2257-2262.
- <sup>25</sup> Paul, S.; Neese, F.; Pantazis, D.A. Structural models of the biological oxygen-evolving complex: achievements, insights, and challenges for biomimicry. *Green Chem.* **2017**, *19*, 2309-2325.
- <sup>26</sup> (a) Koumoussi, E. S.; Mukherjee, S.; Beavers, C. M.; Teat, S. J.; Christou, G.; Stamatatos, T. C. Towards models of the oxygen-evolving complex (OEC) of photosystem II: a Mn<sub>4</sub>Ca cluster of relevance to low oxidation states of the OEC. *Chem. Commun.* **2011**, *47*, 11128-11130. (b) Alaimo, A.A.; Takahashi, D.; Cunha-Silva, L.; Christou, G.; Stamatatos, T.C. Emissive {Mn<sub>4</sub>Ca} Clusters with Square Pyramidal Topologies: Syntheses and Structural, Spectroscopic, and Physicochemical Characterization. *Inorg. Chem.* **2015**, *54*, 2137-2151.
- <sup>27</sup> For some representative references, see: (a) Zaleski, C. M.; Kampf, J. W.; Mallah, T.; Kirk, M. L.; Pecoraro, V. L. Assessing the Slow Magnetic Relaxation Behavior of Ln<sup>III</sup><sub>4</sub>Mn<sup>III</sup><sub>6</sub> Metallacrowns. *Inorg. Chem.* **2007**, *46*, 1954-1956. (b) Boron III, T. T.; Kampf, J. W.; Pecoraro,

---

V. L. A Mixed 3d-4f 14-Metallacrown-5 Complex That Displays Slow Magnetic Relaxation through Geometric Control of Magnetoanisotropy. *Inorg. Chem.* **2010**, *49*, 9104-9106. (c) Zaleski, C. M.; Depperman, E. C.; Kampf, J. W.; Kirk, M. L.; Pecoraro, V. L. Synthesis, Structure, and Magnetic Properties of a Large Lanthanide–Transition-Metal Single-Molecule Magnet. *Angew. Chem. Int. Ed.* **2004**, *43*, 3912-3914. (d) Deb, A.; Boron III, T. T.; Itou, M.; Sakurai, Y.; Mallah, T.; Pecoraro, V. L.; Penner-Hahn, J. E. Understanding Spin Structure in Metallacrown Single-Molecule Magnets using Magnetic Compton Scattering. *J. Am. Chem. Soc.* **2014**, *136*, 4889-4892. (e) Chow, C. Y.; Trivedi, E. R.; Pecoraro, V.; Zaleski, C. M. Heterometallic Mixed 3d-4f Metallacrowns: Structural Versatility, Luminescence, and Molecular Magnetism. *Comments Inorg. Chem.* **2015**, *35*, 214-253.

<sup>28</sup> Diethelm, R.; Miller, M. G.; Shibles R.; Stewart, C. R. Effect of Salicylhydroxamic Acid on Respiration, Photosynthesis, and Peroxidase Activity in Various Plant Tissues. *Plant Cell Physiol.* **1990**, *31*, 179-185.

<sup>29</sup> (a) Vincent, J. B.; Chang, H.- R.; Folting, K.; Huffman, J. C.; Christou, G.; Hendrickson, D. N. Preparation and Physical Properties of Trinuclear Oxo-Centered Manganese Complexes of the General Formulation  $[\text{Mn}_3\text{O}(\text{O}_2\text{CR})_6\text{L}_3]^{0,+}$  (R = Me or Ph; L = a Neutral Donor Group) and the Crystal Structures of  $[\text{Mn}_3\text{O}(\text{O}_2\text{CMe})_6(\text{pyr})_3](\text{pyr})$  and  $[\text{Mn}_3\text{O}(\text{O}_2\text{CPh})_6(\text{pyr})_2(\text{H}_2\text{O})]\cdot 0.5\text{MeCN}$ . *J. Am. Chem. Soc.* **1987**, *109*, 5703-5711. (b) Wemple, M. W.; Tsai, H. -L.; Wang, S.; Claude, J. P.; Streib, W. E.; Huffman, J. C.; Hendrickson, D. N.; Christou, G. Tetranuclear and Octanuclear Manganese Carboxylate Clusters: Preparation and Reactivity of  $(\text{NBu}^n_4)[\text{Mn}_4\text{O}_2(\text{O}_2\text{CPh})_9(\text{H}_2\text{O})]$  and Synthesis of  $(\text{NBu}^n_4)[\text{Mn}_8\text{O}_4(\text{O}_2\text{CPh})_{12}(\text{Et}_2\text{mal})_2(\text{H}_2\text{O})_2]$  with a “Linked-Butterfly” Structure. *Inorg. Chem.* **1996**, *35*, 6437-6449.

<sup>30</sup> Rigaku/MS. *CrystalClear*. Rigaku/MS Inc.; The Woodlands, TX, 2005.



- 
- <sup>31</sup> Sheldrick, G. M. *SHELXS-97*, Program for Crystal Structure Solution; University of Göttingen, 1997.
- <sup>32</sup> Sheldrick, G. M. Crystal structure refinement with SHELXL. *Acta Cryst.* **2015**, *C71*, 3-8.
- <sup>33</sup> Kottke, T.; Stalke, D. Crystal handling at low temperatures. *J. App. Cryst.* **1993**, *26*, 615-619.
- <sup>34</sup> *APEX2*, Data Collection Software Version 2.1-RC13; Bruker AXS: Delft, The Netherlands 2006.
- <sup>35</sup> *Cryopad*, Remote Monitoring and Control, Version 1.451; Oxford Cryosystems: Oxford, United Kingdom, 2006.
- <sup>36</sup> *SAINT+*, Data Integration Engine v. 7.23a ©; Bruker AXS: Madison, WI, 1997-2005.
- <sup>37</sup> Sheldrick, G. M. *SADABS*, 2012/1, Bruker AXS Area Detector Scaling and Absorption Correction Program; 2012, Bruker AXS: Madison, WI.
- <sup>38</sup> Sheldrick, G. M. A short history of *SHELX*. *Acta Cryst. A* **2008**, *64*, 112-122.
- <sup>39</sup> Sheldrick, G. M. *SHELXT*, v. 2014/3, Program for Crystal Structure Solution; University of Göttingen, 2014.
- <sup>40</sup> Sheldrick, G. M. *SHELXL*, v. 2014, Program for Crystal Structure Refinement; University of Göttingen, 2014.
- <sup>41</sup> (a) Spek, A. L. PLATON, An Integrated Tool for the Analysis of the Results of a Single Crystal Structure Determination. *Acta Cryst. A* **1990**, *46*, C34. (b) Spek, A. L. Single-crystal structure validation with the program PLATON. *J. Appl. Crystallogr.* **2003**, *36*, 7-13. (c) van der Sluis, P.; Spek, A. L. BYPASS: an effective method for the refinement of crystal structures containing disordered solvent regions. *Acta Cryst. A* **1990**, *46*, 194-201. (d) *Mercury*; Bruno, I. J.; Cole, J. C.; Edgington, P. R.; Kessler, M. K.; Macrae, C. F.; McCabe, P.; Pearson, J.; Taylor, R. New software for searching the Cambridge Structural Database and visualizing crystal

---

structures. *Acta Crystallogr., Sect. B: Struct. Sci.* **2002**, *58*, 389-397. (e) Bradenburg, K. *DIAMOND*, Release 3.1f; Crystal Impact GbR: Bonn, Germany, 2008.

<sup>42</sup> Bain, G. A.; Berry, J. F. Diamagnetic Corrections and Pascal's Constants. *J. Chem. Educ.* **2008**, *85*, 532-536.

<sup>43</sup> (a) Brechin, E. K.; Soler, M.; Davidson, J.; Hendrickson, D. N.; Parsons, S.; Christou, G. A new class of single-molecule magnet:  $[\text{Mn}_9\text{O}_7(\text{OAc})_{11}(\text{thme})(\text{py})_3(\text{H}_2\text{O})_2]$  with an  $S = 17/2$  ground state. *Chem. Commun.* **2002**, 2252–2253. (b) Brechin, E. K.; Soler, M.; Christou, G.; Helliwell, M.; Teat, S. J.; Wernsdorfer, W. Dodecanuclear and octanuclear manganese rods. *Chem. Commun.* **2003**, 1276–1277.

<sup>44</sup> (a) Mazarakioti, E. C.; Poole, K. M.; Cunha-Silva, L.; Christou, G.; Stamatatos, T. C. A new family of  $\text{Ln}_7$  clusters with an ideal  $D_{3h}$  metal-centered trigonal prismatic geometry, and SMM and photoluminescence behaviors. *Dalton Trans.* **2014**, *43*, 11456–11460. (b) Hooper, T. N.; Inglis, R.; Palacios, M. A.; Nichol, G. S.; Pitak, M. B.; Coles, S. J.; Lorusso, G.; Evangelisti, M.; Brechin, E. K.  $\text{CO}_2$  as a reaction ingredient for the construction of metal cages: a carbonate-pannelled  $[\text{Gd}_6\text{Cu}_3]$  tridiminished icosahedron. *Chem. Commun.* **2014**, *50*, 3498-3500.

<sup>45</sup> Khairy, E. M.; Shoukry, M. M.; Khalil, M. M.; Mohamed, M. M. A. Metal complexes of salicylhydroxamic acid: equilibrium studies and synthesis. *Trans. Met. Chem.* **1996**, *21*, 176-180. (b) Hall, M. D.; Failes, T. W.; Hibbs, D. E.; Hambley, T. W. Structural Investigations of Palladium(II) and Platinum(II) Complexes of Salicylhydroxamic Acid. *Inorg. Chem.* **2002**, *41*, 1223-1228.

<sup>46</sup> Deacon, G. B.; Phillips, R. J. Relationships between the carbon-oxygen stretching frequencies of carboxylato complexes and the type of carboxylate coordination. *Coord. Chem. Rev.* **1980**, *33*, 227-250.

- 
- <sup>47</sup> Glazunov, V. P.; Mashkovsky, A. A.; Odinkov, S. E. Infrared spectroscopic study of interionic hydrogen bonds in triethylammonium salts. *J. Chem. Soc., Faraday Trans. 2* **1979**, *75*, 629-635.
- <sup>48</sup> (a) Langley, S. K.; Moubaraki, B.; Murray, K. S. Magnetic Properties of Hexanuclear Lanthanide(III) Clusters Incorporating a Central  $\mu_6$ -Carbonate Ligand Derived from Atmospheric CO<sub>2</sub> Fixation. *Inorg. Chem.* **2012**, *51*, 3947-3949. (b) Dermizaki, D.; Lorusso, G.; Raptopoulou, C. P.; Psycharis, V.; Escuer, A.; Evangelisti, M.; Perlepes, S. P.; Stamatatos, T. C. Molecular Nanoscale Magnetic Refrigerants: A Ferrimagnetic {Cu<sup>II</sup><sub>15</sub>Gd<sup>III</sup><sub>7</sub>} Cagelike Cluster from the Use of Pyridine-2,6-dimethanol. *Inorg. Chem.* **2013**, *52*, 10235-10237.
- <sup>49</sup> Liu, W.; Thorp, H. H. Bond Valence Sum Analysis of Metal-Ligand Bond Lengths in Metalloenzymes and Model Complexes. 2. Refined Distances and Other Enzymes. *Inorg. Chem.* **1993**, *32*, 4102-4105.
- <sup>50</sup> For an excellent review on metallocrowns and their nomenclature, see: Pecoraro, V. L.; Stemmler, A. J.; Gibney, B. P.; Bodwin, J.; Kampf, J. W.; Wang, H. Metallocrowns: A New Class of Molecular Recognition Agents. In *Prog. Inorg. Chem*; Karlin, K. D., Ed.; John Wiley & Sons, Inc., Hoboken, **1996**; Vol. 45, Chapter 2, pp. 83.
- <sup>51</sup> Addison, A. W.; Rao, T. N.; Reedijk, J.; van Rijn, J.; Verschoor, G. C. Synthesis, structure, and spectroscopic properties of copper(II) compounds containing nitrogen-sulphur donor ligands; the crystal and molecular structure of aqua[1,7-bis(*N*-methylbenzimidazol-2'-yl)-2,6-dithiaheptane]copper(II) perchlorate. *J. Chem. Soc., Dalton Trans.* **1984**, 1349-1356.
- <sup>52</sup> Zabrodsky, H.; Peleg, S.; Avnir, D. Continuous Symmetry Measures. 2. Symmetry Groups and the Tetrahedron. *J. Am. Chem. Soc.* **1993**, *115*, 8278-8289.

- 
- <sup>53</sup> Alvarez, S.; Alemany, P.; Casanova, D.; Cirera, J.; Llunell, M.; Avnir, D. Shape maps and polyhedral interconversion paths in transition metal chemistry. *Coord. Chem. Rev.* **2005**, *249*, 1693-1708.
- <sup>54</sup> Siegbahn, P. E. M. Water oxidation mechanism in photosystem II, including oxidations, proton release pathways, O–O bond formation and O<sub>2</sub> release. *Biochim. Biophys. Acta.* **2013**, *1827*, 1003–1019.
- <sup>55</sup> Kanady, J.S.; Lin, P.- H.; Carsch, K. M.; Nielsen, R. J.; Takase, M .K.; Goddard III, W. A.; Agapie, T. Toward Models for the Full Oxygen-Evolving Complex of Photosystem II by Ligand Coordination To Lower the Symmetry of the Mn<sub>3</sub>CaO<sub>4</sub> Cubane: Demonstration That Electronic Effects Facilitate Binding a Fifth Metal. *J. Am. Chem. Soc.* **2014**, *136*, 14373-14376.
- <sup>56</sup> Tsui, E. Y.; Tran, R.; Yano, J.; Agapie, T. Redox-inactive metals modulate the reduction potential in heterometallic manganese-oxido clusters. *Nat. Chem.* **2013**, *5*, 293-299.
- <sup>57</sup> Nayak, S.; Nayek, H. P.; Dehnen, S.; Powell, A. K.; Reedijk, J. Trigonal propeller-shaped [Mn<sup>III</sup><sub>3</sub>M<sup>II</sup>Na] complexes (M = Mn, Ca): structural and functional models for the dioxygen evolving centre of PSII. *Dalton Trans.* **2011**, *40*, 2699-2702.
- <sup>58</sup> Mishra, A.; Wernsdorfer, W.; Abboud, K. A.; Christou, G. The first high oxidation state manganese-calcium cluster: relevance to the water oxidizing complex of photosynthesis. *Chem. Commun.* **2005**, 54-56.
- <sup>59</sup> Kotzabasaki, V.; Siczek, M.; Lis, T.; Milios, C. J. The first heterometallic Mn-Ca cluster containing exclusively Mn(III) centers. *Inorg. Chem. Commun.* **2011**, *14*, 213-216.
- <sup>60</sup> Hewitt, I. J.; Tang, J.- K.; Madhu, N. T.; Clerac, R.; Buth, G.; Anson, C. E.; Powell, A. K. A series of new structural models for the OEC in photosystem II. *Chem. Commun.* **2006**, 2650-2652.

- 
- <sup>61</sup> Fuller, R. O.; Koutsantonis, G. A.; Lozic, I.; Ogden, M. I.; Skelton, B. W. Manganese-calcium cluster supported by calixarenes. *Dalton Trans.* **2015**, *44*, 2132-2137.
- <sup>62</sup> Li, N.; Wang, M.; Ma, C.- B.; Hu, M.- Q.; Zhou, R.- W.; Chen, H.; Chen, C.- N. Synthesis and characterization of a new 2D trimetallic Mn/Ca/Na complex. *Inorg. Chem. Commun.* **2010**, *13*, 730-732.
- <sup>63</sup> Martin-Diaconescu, V.; Gennari, M.; Gerey, B.; Tsui, E.; Kanady, J.; Tran, R.; Pécaut, J.; Maganas, D.; Krewald, V.; Gouré, E.; Duboc, C.; Yano, J.; Agapie, T.; Collomb, M.- N.; DeBeer, S. Ca K-Edge XAS as a Probe of Calcium Centers in Complex Systems. *Inorg. Chem.* **2015**, *54*, 1283-1292.
- <sup>64</sup> Wang, W.; Zhang, X.; Chen, F.; Ma, C.; Chen, C.; Liu, Q.; Liao, D.; Li, L. Homo- and hetero-metallic manganese citrate complexes: Syntheses, crystal structures and magnetic properties. *Polyhedron* **2005**, *24*, 1656-1668.
- <sup>65</sup> Chen, C.; Zhang, C.; Dong, H.; Zhao, J. Artificial synthetic Mn<sup>IV</sup>Ca-oxido complexes mimic the oxygen-evolving complex in photosystem II. *Dalton Trans.* **2015**, *44*, 4431-4435.
- <sup>66</sup> Jerzykiewicz, L. B.; Utko, J.; Duczmal, M.; Sobota, P. Syntheses, structure, and properties of a manganese-calcium cluster containing a Mn<sub>4</sub>Ca<sub>2</sub> core. *Dalton Trans.* **2007**, 825-826.
- <sup>67</sup> Benniston, A. C.; Melnic, S.; Turta, C.; Arauzo, A. B.; Bartolomé, J.; Bartolomé, E.; Harrington, R. W.; Probert, M. R. Preparation and properties of a calcium(II)-based molecular chain decorated with manganese(II) butterfly-like complexes. *Dalton Trans.* **2014**, *43*, 13349-13357.
- <sup>68</sup> Escriche-Tur, L.; Jover, J.; Font-Bardia, M.; Aullón, G.; Corbella, M. Magnetic Behavior of Heterometallic Wheels Having a [Mn<sup>IV</sup><sub>6</sub>M<sub>2</sub>O<sub>9</sub>]<sup>10+</sup> Core with M = Ca<sup>2+</sup> and Sr<sup>2+</sup>. *Inorg. Chem.* **2015**, *54*, 11596-11605.

---

<sup>69</sup> For example, see: (a) Koumoussi, E. S.; Raptopoulou, C. P.; Perlepes, S. P.; Escuer, A.; Stamatatos, T. C. Strong antiferromagnetic coupling in doubly *N,O* oximate-bridged dinuclear copper(II) complexes. *Polyhedron* **2010**, *29*, 204-211. (b) Pringouri, K. V.; Raptopoulou, C. P.; Escuer, A.; Stamatatos, T. C. Initial use of di-2-pyridyl ketone oxime in chromium carboxylate chemistry: Triangular  $\{\text{Cr}^{\text{III}}_3(\mu_3\text{-O})\}^{7+}$  compounds and unexpected formation of a carboxylate-free dichromium(II,II) complex. *Inorg. Chim. Acta* **2007**, *360*, 69-83. (c) Verani, C. N.; Bothe, E.; Burdinski, D.; Weyhermüller, T.; Flörke, U.; Chaudhuri, P. Synthesis, Structure, Electrochemistry, and Magnetism of  $[\text{Mn}^{\text{III}}\text{Mn}^{\text{III}}]$ ,  $[\text{Mn}^{\text{III}}\text{Fe}^{\text{III}}]$  and  $[\text{Fe}^{\text{III}}\text{Fe}^{\text{III}}]$  Species. *Eur. J. Inorg. Chem.* **2001**, 2161-2169. (d) Gass, I. A.; Milios, C. J.; Collins, A.; White, F. J.; Budd, L.; Parsons, S.; Murrie, M.; Perlepes, S. P.; Brechin, E. K. Polymetallic clusters of iron(III) with derivatised salicylaldoximes. *Dalton Trans.* **2008**, 2043-2053.

<sup>70</sup> Chilton, N. F.; Anderson, R. P.; Turner, L. D.; Soncini, A.; Murray, K. S. PHI: A Powerful New Program for the Analysis of Anisotropic Monomeric and Exchange-Coupled Polynuclear *d*- and *f*-block Complexes. *J. Comput. Chem.* **2013**, *34*, 1164-1175.

<sup>71</sup> (a) Beck, W. F.; Brudvig, G. W. Reactions of hydroxylamine with the electron-donor side of photosystem II. *Biochemistry* **1987**, *26*, 8285-8295. (b) Lin, C.; Brudvig, G. W. Chemical oxidation and reduction of the O<sub>2</sub>-evolution center in Photosystem II. *Photosynth. Res.* **1993**, *38*, 441-448. (c) Riggs-Gelasco, P. J.; Mei, R.; Yocum, C. F.; Penner-Hahn, J. E. Reduced Derivatives of the Mn Cluster in the Oxygen-Evolving Complex of Photosystem II: An EXAFS Study. *J. Am. Chem. Soc.* **1996**, *118*, 2387-2399.

<sup>72</sup> (a) Sarrou, J.; Ioannidis, N.; Deligiannakis, Y.; Petrouleas, V. A Mn(II)–Mn(III) EPR Signal Arises from the Interaction of NO with the S<sub>1</sub> State of the Water-Oxidizing Complex of Photosystem II. *Biochemistry* **1998**, *37*, 3581-3587. (b) Ioannidis, N.; Sarrou, J.; Schansker, G.;

---

Petrouleas, V. NO Reversibly Reduces the Water-Oxidizing Complex of Photosystem II through  $S_0$  and  $S_{-1}$  to the State Characterized by the Mn(II)–Mn(III) Multiline EPR Signal. *Biochemistry* **1998**, *37*, 16445-16451.

<sup>73</sup> (a) Messinger, J.; Wacker, U.; Renger, G. Unusual Low Reactivity of the Water Oxidase in Redox State  $S_3$  toward Exogenous Reductants. Analysis of the  $NH_2OH$ - and  $NH_2NH_2$ -Induced Modifications of Flash-Induced Oxygen Evolution in Isolated Spinach Thylakoids. *Biochemistry*, **1991**, *30*, 7852-7862. (b) Bösing, P.; Willner, A.; Pape, T.; Heppa, A.; Mitzel, N. W. Structural diversity in bishydroxylamine complexes of gallium. *Dalton Trans.* **2008**, 2549-2556. (c) Kuntzleman, T.; Yocum, C. F. Reduction-Induced Inhibition and Mn(II) Release from the Photosystem II Oxygen-Evolving Complex by Hydroquinone or  $NH_2OH$  Are Consistent with a Mn(III)/Mn(III)/Mn(IV)/Mn(IV) Oxidation State for the Dark-Adapted Enzyme. *Biochemistry* **2005**, *44*, 2129-2142.

<sup>74</sup> Lampropoulos, C.; Thuijs, A. E.; Mitchell, K. J.; Abboud, K. A.; Christou, G. Manganese/Cerium Clusters Spanning a Range of Oxidation Levels and  $CeMn_8$ ,  $Ce_2Mn_4$ , and  $Ce_6Mn_4$  Nuclearities: Structural, Magnetic, and EPR Properties. *Inorg. Chem.* **2014**, *53*, 6805-6816.

---

## Table of Contents

The employment of salicylhydroxamic acid in heterometallic Mn-Ca chemistry has afforded four new cluster compounds with diverse structural topologies, metal stoichiometries, and oxidation state descriptions.

